

Infrared Multiple Photon Dissociation Action Spectroscopy of Deprotonated RNA Mononucleotides: Gas-Phase Conformations and Energetics

Y.-w. Nei,[†] K. T. Crampton,[†] G. Berden,[‡] J. Oomens,^{‡,§} and M. T. Rodgers*,[†]

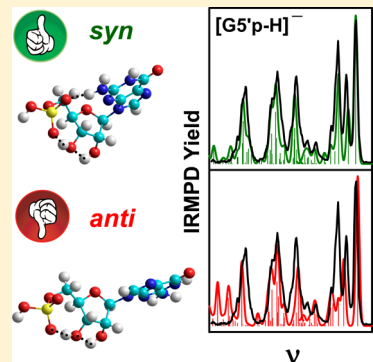
[†]Department of Chemistry, Wayne State University, Detroit, Michigan 48202, United States

[‡]Radboud University Nijmegen, Institute for Molecules and Materials, FELIX Facility, Toernooiveld 7, 6525ED Nijmegen, The Netherlands

[§]van't Hoff Institute for Molecular Sciences, University of Amsterdam, Amsterdam, The Netherlands

S Supporting Information

ABSTRACT: The IRMPD action spectra of the deprotonated forms of the four common RNA mononucleotides, adenosine-5'-monophosphate (A5'p), guanosine-5'-monophosphate (G5'p), cytidine-5'-monophosphate (C5'p), and uridine-5'-monophosphate (U5'p), are measured to probe their gas-phase structures. The IRMPD action spectra of all four deprotonated RNA mononucleotides exhibit distinct IR signatures in the frequency region investigated, 570–1900 cm⁻¹, that allows these deprotonated mononucleotides to be easily differentiated from one other. Comparison of the measured IRMPD action spectra to the linear IR spectra calculated at the B3LYP/6-31+G(d,p) level of theory finds that the most stable conformations of the deprotonated forms of A5'p, C5'p, and U5'p are accessed in the experiments, and these conformers adopt the C3' *endo* conformation of the ribose moiety and the *anti* conformation of the nucleobase. In the case of deprotonated G5'p, the most stable conformer is also accessed in the experiments. However, the ground-state conformer differs from the other three deprotonated RNA mononucleotides in that it adopts the *syn* rather than *anti* conformation for the nucleobase. Present results are compared to results previously obtained for the deprotonated forms of the four common DNA mononucleotides to examine the fundamental conformational differences between these species, and thus elucidate the effects of the 2'-hydroxyl group on their structure, stability, and fragmentation behavior.



INTRODUCTION

The most common features that distinguish DNA and RNA structures are the double helical structure adopted by DNA, the 2'-hydroxyl group of the ribose moiety of RNA, and the replacement of thymine by uracil in RNA, which can also be viewed as methylation of uracil in DNA. In comparison, DNA is more important in the central dogma of molecular biology than RNA. Therefore, it is important for DNA to adopt the double helical structure to prevent modification and mutation of the nucleobase and ribosyl moieties, and to provide a complementary back up copy of the genetic information. The 2'-hydroxyl group of the ribose moiety of RNA changes the chemical properties of the nucleotides as the 2'-hydroxyl group is susceptible to hydrolysis, provides an additional site for hydrogen bonding or ligation upon binding of metal ions to both the 2'- and 3'-hydroxyl groups,¹ and enables the formation of 2',3'-cyclic diester structures.² Methylation is used by chemists, biologists, and even nature to change the chemical properties of molecules, most often as a protecting group but occasionally as an activating group.^{3–6} As a result of these differences, it is not surprising that RNA nucleotides are found to play more biological roles than DNA nucleotides, beside their primary roles in passing on genetic information. Most of

these biological functions are carried out by more complex RNA nucleotides rather than the simple mononucleotides themselves. However, RNA mononucleotides do play important roles. For example, adenosine-5'-triphosphate (ATP) and adenosine-5'-diphosphate (ADP) are the energy carriers in cells where free energy is released through the hydrolysis of the phosphodiester bond. The adenine nucleotide is also a component of many enzyme cofactors such as coenzyme A, nicotinamide adenine dinucleotide (NAD⁺), nicotinamide adenine dinucleotide phosphate (NADP⁺), and flavin adenine dinucleotide (FAD). RNA mononucleotides that are more well-known for their biological functions include 3',5'-cyclic adenosine monophosphate (cAMP) and 3',5'-cyclic guanosine monophosphate (cGMP), where they act as secondary messengers in the intracellular signal transduction of the cell.⁷ Several examples of the lesser known functions of the common RNA mononucleotides include adenosine-5'-monophosphate activated protein kinase that regulates the production of ATP,⁸ cytidine-5'-monophosphate induced conformational change to

Received: April 21, 2013

Revised: September 19, 2013

Published: September 22, 2013

the enzyme sialytransferase that catalyzes the synthesis of sialic acid containing oligosaccharides,⁹ application of zirconium uridine-5'-monophosphate complexes as an electrochemistry probe of myoglobin,¹⁰ and the inhibition of the hydrolase enzyme, sphingomyelinase, which is required in the sphingolipid metabolism reaction by adenosine-5'-monophosphate.¹¹

Since the coupling of mass spectrometry and high-powered wavelength-tunable free electron lasers for infrared multiple photon dissociation (IRMPD) experiments,^{12–17} combined with the dramatic improvement and generalization of supercomputing systems, many studies have sought to provide information regarding the conformational structure of biologically relevant molecules using their unique bending and stretching modes in the mid-IR fingerprint region.^{18–28} In particular, studies related to nucleic acids have been an active area of interest. The IR spectra in the mid-IR region have been reported for nucleobases,^{17,29,30} modified nucleobases,^{30–32} and proton-bound dimers of nucleobases^{33,34} in the gas phase. Spectra in the same frequency region have also been obtained for the deprotonated and protonated forms of cAMP,³⁵ and complexation of Pb²⁺ with the deprotonated forms of 2'-deoxycytidine-5'-monophosphate, cytidine-5'-monophosphate,³⁶ and uridine-5'-monophosphate.³⁷ Furthermore, studies of large oligonucleotides such as G-quadruplexes³⁸ and the cytosine-rich DNA i-motif³⁹ have also been reported.

Recently, the first systematic studies of the deprotonated forms of all four common DNA mononucleotides via IRMPD action spectroscopy and high level theoretical calculations were reported by our laboratory⁴⁰ in an attempt to better understand their conformations in the absence of an ensemble solvent system, and as a first step in a broader program of study aimed at understanding the effects of pH, metal-ion content, nucleobase modification, and the presence of different ligands and counterions on the structures of nucleotides that typically exist in normal physiological environments. To elucidate the effects of the 2'-hydroxyl group and demethylation of the thymine nucleobase, our studies of the deprotonated DNA mononucleotides are expanded here to include the determination of the conformations of the deprotonated RNA mononucleotides using the same IRMPD action spectroscopy techniques and electronic structure theory methods. In the present work, the structures and IR spectra of the four common RNA mononucleotides in their deprotonated forms are examined including adenosine-5'-monophosphate (A5'p), guanosine-5'-monophosphate (G5'p), cytidine-5'-monophosphate (C5'p), and uridine-5'-monophosphate (U5'p), as shown in Figure 1.

EXPERIMENTAL AND COMPUTATIONAL SECTION

IRMPD Action Spectroscopy. IRMPD action spectra of the deprotonated forms of the four common RNA mononucleotides (X5'p) were measured using a 4.7 T Fourier transform ion cyclotron resonance mass spectrometer (FT-ICR MS) coupled to the FELIX free electron laser (FEL) that has been described in detail elsewhere.^{13,41,42} The mononucleotide precursors, adenosine-5'-monophosphate monohydrate, guanosine-5'-monophosphate disodium salt hydrate, and uridine-5'-monophosphate, were obtained from Sigma Aldrich, whereas cytidine-5'-monophosphate was obtained from Tokyo Chemical Industry (TCI) and used without further purification. The deprotonated forms of each RNA mononucleotide were generated using a Micromass “Z-spray” electrospray ionization (ESI) source from solutions containing 1–2 mM of the RNA

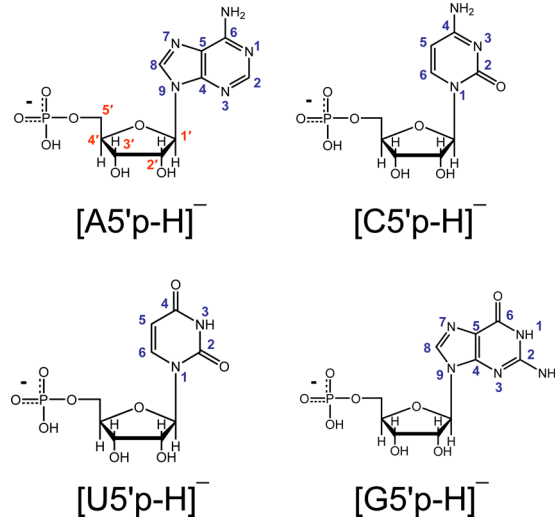


Figure 1. Structures of deprotonated RNA mononucleotides $[X5'p-H]^-$, where X5'p = adenosine-5'-monophosphate (A5'p), cytidine-5'-monophosphate (dC5'p), guanosine-5'-monophosphate (G5'p), and uridine-5'-monophosphate (U5'p).

mononucleotide in an approximately 50%:50% MeOH:H₂O mixture. The analyte solution was delivered to the electrospray needle at a flow rate of 10 μ L/min, and the voltage was held at approximately -2 kV to assist in the charging and desolvation of the analyte mononucleotides. Ions emanating from the ESI source were accumulated in a hexapole trap for several seconds, pulse extracted through a quadrupole bender, and injected into the ICR cell by an rf octopole ion guide. During ion injection into the ICR cell, a pulsed positive dc bias was applied to the octopole with relative ground potential on the ICR cell such that the excess kinetic energy of the ions was decreased by climbing the potential barrier, enabling facile capture of the ions by gated trapping in the ICR cell without collisional cooling. This dc bias switching method is described in detail elsewhere.⁴¹ The deprotonated RNA mononucleotide was mass selected using stored waveform inverse Fourier transform (SWIFT) techniques and irradiated by the FEL at pulse energies of \sim 40 mJ per macropulse of 5 μ s duration at a repetition rate of 10 Hz for 3–4 s, corresponding to interaction with 30–40 macropulses over the wavelength range extending from \sim 17.5 μ m (571 cm^{-1}) to 5.3 μ m (1887 cm^{-1}).

Computational Details. Due to the conformational flexibility of the deprotonated RNA mononucleotides, simulated annealing was first carried out to search for low-energy candidate structures, and followed by high level density functional theory (DFT) and *ab initio* calculations. The annealing process is carried out using HyperChem software⁴³ with the Amber force field. Initial structures of each deprotonated RNA mononucleotide are subjected to 300 cycles of simulated annealing, where each cycle involves 0.3 ps of thermal heating from 0 to 1000 K, the simulation temperature. The deprotonated RNA mononucleotide is then allowed to sample conformational space at the simulation temperature for 0.2 ps. The system is then gradually cooled down to 0 K over a period of 0.3 ps. The resulting conformation of the RNA mononucleotide is then optimized to a local minimum. A molecular mechanics calculation is performed every 0.001 ps in each cycle, and a snapshot of the lowest energy structure found at the end of each cycle is saved and used to initiate the subsequent cycle. All structures within

50 kJ/mol of the most stable structure computed, as well as additional plausible conformers that chemical intuition suggests might be important, were optimized and harmonic vibrational frequencies calculated at the B3LYP/6-311+G(d,p) level of theory using the Gaussian 09 suite of programs.⁴⁴ Single-point energy calculations were initially carried out at the B3LYP/6-311+G(2d,2p) level of theory on all optimized structures to identify low-energy conformers and to reduce computational cost. Single-point energies of all conformers found that lie within 15 kJ/mol of the ground-state conformer for each deprotonated RNA mononucleotide at this level of theory were then also calculated at the B3P86, M06, and MP2(full) levels of theory using the 6-311+G(2d,2p) basis set to examine the structural and energetic trends among the various low-energy conformations and to evaluate the strengths and weaknesses in each theory. Relative enthalpies and Gibbs free energies at 298 K for each level of theory were determined by including zero-point vibrational energy (ZPE) and thermal corrections calculated at the B3LYP/6-311+G(d,p) level of theory. In the previous theoretical and IRMPD studies of phosphorylated species,^{23,40,45,46} unscaled theoretical harmonic frequencies were found to provide the best match to the P=O and P—O stretching modes. However, even without scaling, several spectral features attributed to the modes of the phosphate moiety are still red-shifted as compared to the measured frequencies for these vibrational modes. Therefore, two different scaling factors, 0.978 for frequencies above 1300 cm⁻¹ (shown in blue in the computed spectra) and 1.00 for frequencies below 1300 cm⁻¹ (shown in red in the computed spectra), are applied to the calculated harmonic frequencies and used along with the calculated single-photon IR absorption intensities to generate theoretical linear IR spectra. Before comparison with the measured IRMPD spectra, the calculated vibrational spectra are convoluted with a 20 cm⁻¹ fwhm Gaussian line shape.

RESULTS AND DISCUSSION

IRMPD Action Spectra. In all cases, the dominant IRMPD pathway of the deprotonated RNA mononucleotides, [X5'p-H]⁻, is the cleavage of the phosphate ester (P—OC) bond resulting in the formation of the metaphosphate anion, PO₃⁻. Phosphate ester bond (PO—C) cleavage resulting in formation of the dihydrogen phosphate ion, [H₂PO₄]⁻, glycosidic bond cleavage resulting in loss of the neutral nucleobase (Nuc), and the formation of the deprotonated dehydrated ribose monophosphate moiety, [X5'p-Nuc-H]⁻, are observed as minor dissociation pathways. The deprotonated nucleobase anions were not observed in the current experiments, whereas these species were observed as very minor dissociation products upon IRMPD of the deprotonated DNA mononucleotides.⁴⁰ An energy resolved CID study of [A5'p-H]⁻ by Kebarle and co-workers⁴⁷ found that the fragmentation pathway leading to formation of deprotonated adenine, [Ade-H]⁻, lies 0.31–1.24 eV higher in energy than the other three dissociation pathways observed here. Several investigations of UV photodissociation of [A5'p-H]⁻ and [G5'p-H]⁻ also observed low abundance of the deprotonated nucleobase anions in their mass analysis.^{48–50} These differences between the DNA and RNA mononucleotides suggest that the 2'-hydroxyl increases the activation energy for glycosidic bond cleavage of the deprotonated mononucleotides.

An IRMPD yield is calculated from the precursor ion intensity (I_p) and the sum of the fragment ion intensities (I_f_i) after laser irradiation at each frequency, as shown in eq 1.

$$\text{IRMPD yield} = \frac{\sum_i I_{f_i}}{I_p + \sum_i I_{f_i}} \quad (1)$$

An IRMPD action spectrum is obtained by plotting the IRMPD yield as a function of the FEL laser frequency. Due to the variation in the laser power of the FEL with wavelength, the IRMPD yields were normalized linearly with laser power.

IRMPD spectra were obtained for the deprotonated forms of the four common RNA mononucleotides, [A5'p-H]⁻, [C5'p-H]⁻, [U5'p-H]⁻, and [G5'p-H]⁻, over the range from ~571 to 1887 cm⁻¹. The measured IRMPD action spectra of these species along with the previously reported IRMPD spectrum of deprotonated diethyl phosphate, [DEP-H]⁻,⁴⁵ are compared in Figure 2. As can be seen in the figure, unique spectral features

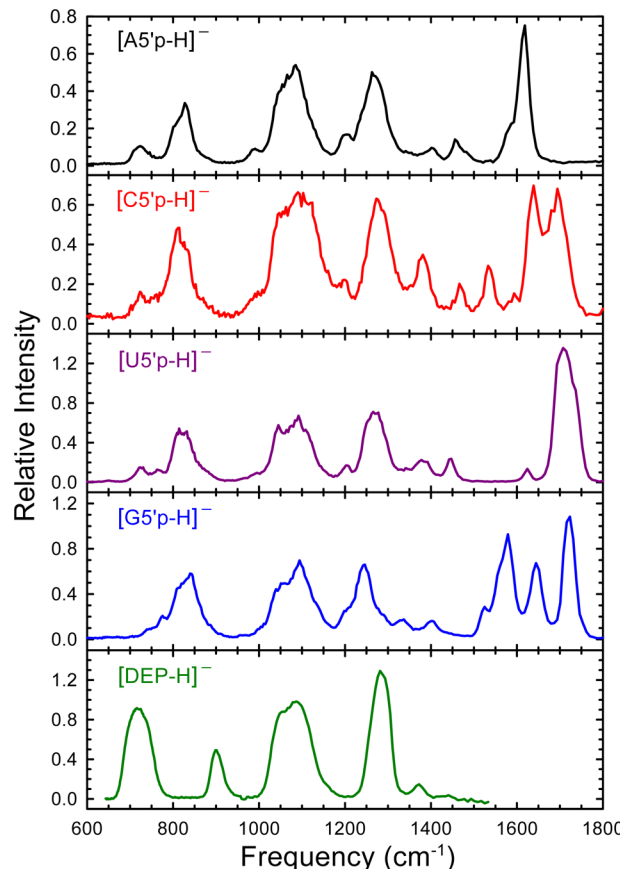


Figure 2. Infrared multiple photon dissociation action spectra of the deprotonated RNA mononucleotides, [X5'p-H]⁻, and deprotonated diethyl phosphate, [DEP-H]⁻. Results for [DEP-H]⁻ are taken from ref 45.

are observed in each spectrum that allow these ions to be easily differentiated from one another, most notably the bands extending from 1400 to 1800 cm⁻¹. The presence of a sharp peak at ~1670–1770 cm⁻¹ in the IRMPD action spectra of [C5'p-H]⁻, [U5'p-H]⁻, and [G5'p-H]⁻ but absent in the IRMPD action spectrum of [A5'p-H]⁻ suggests that these bands likely arise from the carbonyl stretching modes of these nucleobases. Similarly, the appearance of an intense band at ~1600–1650 cm⁻¹ in the IRMPD action spectra of [A5'p-H]⁻,

$[C5'p\text{-H}]^-$, and $[G5'p\text{-H}]^-$, that is of very low intensity in the spectrum of $[U5'p\text{-H}]^-$, may be due to the intense NH_2 scissoring absorption band that generally appears in this region. The peaks at 715, 1080, and 1280 cm^{-1} in the IRMPD action spectrum of $[\text{DEP-H}]^-$ were assigned to the asymmetric P—O stretching and symmetric and asymmetric stretching of the P—O bonds, respectively.⁴⁵ The IRMPD action spectra of the four $[X5'p\text{-H}]^-$ ions exhibit broad bands that are similar to those characteristic of the phosphate modes of $[\text{DEP-H}]^-$ in the region extending from ~ 650 to 1400 cm^{-1} . However, additional features superimposed on these bands as well as the presence of new spectral features suggests that different mixed character modes other than the bending and stretching modes of the phosphate moiety also contribute. The moderately intense peak in the IRMPD action spectrum of $[\text{DEP-H}]^-$ at $\sim 900\text{ cm}^{-1}$ that arises from stretching of the ethoxy moiety is not observed in the spectra of any of the deprotonated RNA mononucleotides, as expected upon replacement of the ethoxy moiety by the ribose sugar. These comparisons suggest that the bands in the region between ~ 1400 and 1800 cm^{-1} most likely arise from the IR active modes of the nucleobase, while features in the region between 650 and 1400 cm^{-1} are primarily vibrational signatures of the phosphate and ribose moieties, with minor contributions possibly arising from the nucleobase.

Theoretical Results. Similar to the previously reported IRMPD action spectroscopy results for the deprotonated DNA mononucleotides,⁴⁰ the stable low-energy conformations of the deprotonated RNA mononucleotides can generally be distinguished on the basis of the rotation of the nucleobase about the glycosidic bond, and the puckering of the ribose ring. When the nucleobase is oriented toward (away from) the 5' phosphate group and above (away from) the plane of the ribose moiety, defined by $\angle C4'C1'$, the nucleotide adapts the *syn* (or *anti*) conformation, as shown in Figure 3a. Puckering of the ribose ring results in either the C2' or C3' atom being on the same side (*endo*) or opposite side (*exo*) of the plane of the ribose moiety as the C5' atom; see Figure 3b. Furthermore, the stable low-energy conformers that adopt *anti* (or *syn*) and C3' *endo* (or *exo*) conformations can be further distinguished by their $\angle OCS'C4'C3'$ and $\angle POCS'C4'$ dihedral angles, which describe the various orientations that the phosphate moiety and the phosphodiester bond adopt, as listed in Table 1. The orientation of the $\angle OCS'C4'C3'$ dihedral angle is best illustrated by the gauche conformation about the C4'—C5' bond, as shown in Figure 3c, where a positive $\angle OCS'C4'C3'$ dihedral angle indicates that the phosphate ester oxygen atom lies above the C3' atom in the gauche conformation, points above the plane of the ribose moiety defined by $\angle C4'C1'$, and lies on the same side as the nucleobase. In contrast, a negative $\angle OCS'C4'C3'$ dihedral angle suggests that the phosphate ester oxygen atom lies below the C3' atom in the gauche conformation, points downward relative to the plane of the ribose, and on the opposite side of the nucleobase, but lies in or slightly above the plane of the ribose.

Parallel to the previous study of the deprotonated DNA mononucleotides, the ground-state conformers found for $[\text{AS}'p\text{-H}]^-$, $[\text{C5}'p\text{-H}]^-$, and $[\text{U5}'p\text{-H}]^-$ adopt the C3' *endo* conformation of the ribose moiety where the $\angle C1'C2'C3'C4'$ dihedral angle lies in the range between 35.2 and 37.8° and the nucleobase is in the *anti* conformation where the $\angle OC1'N9C4$ dihedral angle for $[\text{AS}'p\text{-H}]^-$ and the $\angle OC1'N9C2$ dihedral angles for $[\text{C5}'p\text{-H}]^-$ and $[\text{U5}'p\text{-H}]^-$ vary between -139.9 and -151.0° . In all three cases, the $\angle OCS'C4'C3'$ dihedral angles

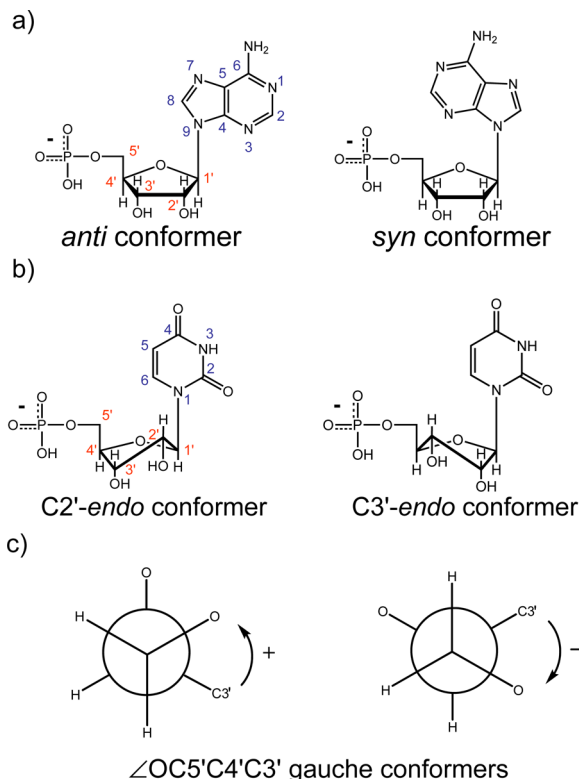


Figure 3. Structural variations in the deprotonated RNA mononucleotides. (a) Rotation of the nucleobase about the glycosidic bond results in the *anti* and *syn* conformations. (b) The puckering of the sugar ring, specifically at the C2' and C3' positions, relative to the plane of the sugar is described as C2' and C3' *endo* and *exo* conformations. (c) Positive and negative $\angle OCS'C4'C3'$ dihedral angle in gauche conformations about the C4'—C5' bond.

are positive and range from 37.3 to 43.3° . Similar to the deprotonated DNA mononucleotides, the $\angle POCS'C4'$ dihedral angles are generally almost of the opposite phase as the $\angle OCS'C4'C3'$ dihedral angles for the ground-state conformers of $[\text{AS}'p\text{-H}]^-$, $[\text{C5}'p\text{-H}]^-$, and $[\text{U5}'p\text{-H}]^-$, and vary from -101.9 to -102.3° . These conformations facilitate hydrogen bond formation between the C3' hydroxyl hydrogen and one of the oxo oxygen atoms. In addition, the 2'-hydroxyl hydrogen atom forms a second intramolecular hydrogen bond to the 3'-hydroxyl oxygen atom. In these conformations, the orientations of the nucleobase and the C5' phosphate ester oxygen atom also suggest that a weak non-canonical hydrogen bonding interaction between the C5'O oxygen and the H6 (or H8) hydrogen atoms of the pyrimidine (or purine) nucleobase provides additional stabilization. These ground-state conformers are designated as the AC3₁ conformers shown in Figures 4–6 and Figure S5 of the Supporting Information. In these conformations, the excess negative charge of the deprotonated phosphate group is stabilized via the intramolecular hydrogen bonding interactions with the 2'- and 3'-hydroxyl groups. These hydrogen bonding interactions also facilitate the puckering of the C3' atom, and induce the flipping of the nucleobase away from the adjacent phosphate moiety to minimize repulsive interactions with the lone pairs of electrons on the functional groups of the nucleobase. In the case of $[\text{G5}'p\text{-H}]^-$, the ground-state conformer adopts the C3' *endo* and *syn* conformations and the $\angle OCS'C4'C3'$ and $\angle POCS'C4'$ dihedral angles are negative and positive,

Table 1. Dihedral Angles (deg) of the Stable Low-Energy Conformers of the Deprotonated RNA Mononucleotides Optimized at the B3LYP/6-31+G(d,p) Level of Theory

complex	conformer	$\angle\text{OC5'}\text{C4'}\text{C3'}$	$\angle\text{POC5'}\text{C4'}$	$\angle\text{C1'}\text{C2'}\text{C3'}\text{C4'}$	$\angle\text{OC1'}\text{N9C4}$	$\angle\text{O}=\text{P}-\text{OC5'}$	$\angle\text{O}=\text{P}-\text{OC5'}$	$\angle\text{O}-\text{P}-\text{OC5'}$	$\angle\text{HO}-\text{P}-\text{O}$
$[\text{A5'}\text{p-H}]^-$	AC3_1	37.3	-102.3	35.2	-139.9	37.2	172.7	-72.8	-85.6
	AC3_2	36.8	-106.1	35.6	-142.9	-84.5	50.4	161.4	92.2
	AC3_1R	36.7	-101.6	35.2	-142.5	36.4	171.1	-72.9	121.3
	AC3_3	-69.3	92.8	28.4	-127.5	-97.8	36.2	151.7	90.2
	AC3_2R	33.7	-107.1	35.8	-146.3	-63.4	70.8	-178.3	-91.4
	AC3_3R	-72.8	96.4	28.3	-128.9	-89.4	45.0	160.2	-82.0
	AC3_4	-88.2	97.5	29.3	-129.4	174.2	-50.2	59.8	90.7
	AC3_5	-72.6	86.5	-6.4	-118.0	-95.2	39.0	154.5	91.3
	AC3_6	-46.4	-66.7	27.2	-122.0	60.4	-164.7	-50.1	-95.4
	AC3_4R	-87.0	96.9	29.5	-131.4	175.0	-50.3	58.7	-129.2
$[\text{C5'}\text{p-H}]^-$	AC3_5R	-75.0	84.7	-8.5	-117.7	-91.0	43.4	158.6	-81.2
	AC3_6R	-46.0	-66.9	27.2	-121.5	60.5	-165.3	-48.9	118.7
	AC3_1	43.3	-102.0	37.8	-151.0	34.5	169.9	-75.9	-84.9
	AC3_1R	43.0	-100.9	37.9	-151.1	31.5	166.3	-78.4	116.0
	AC3_2	40.4	-106.8	37.1	-149.0	-84.1	51.0	162.6	100.3
	AC3_2R	38.3	-108.3	37.5	-152.4	-70.8	63.8	174.5	-96.2
	AC3_3	-67.7	94.4	32.5	-153.6	-98.3	35.8	151.1	90.0
	AC3_3R	-71.9	96.4	32.0	-148.8	-90.2	44.2	159.2	-81.8
	AC3_7	48.9	-104.0	39.1	-157.0	34.5	169.9	-76.2	-84.9
	AC2_1	48.8	140.1	-30.9	-166.4	-178.6	-43.4	68.2	87.6
$[\text{U5'}\text{p-H}]^-$	AC3_7R	48.6	-103.1	39.1	-157.2	32.0	166.8	-78.2	115.1
	AC2_2	51.6	148.5	-30.9	-164.6	-69.2	66.5	179.7	-87.4
	AC3_1	40.6	-101.9	36.0	-144.8	34.6	169.8	-75.6	-85.2
	AC3_1R	40.2	-101.2	36.0	-144.9	33.1	167.7	-76.5	119.6
	AC3_2	39.2	-106.4	36.0	-145.3	-85.0	50.0	161.3	98.4
	AC3_3	-68.6	93.1	27.7	-132.9	-95.3	38.8	154.1	-82.0
	AC3_2R	36.3	-107.7	36.3	-147.6	-65.9	68.3	179.1	-96.8
	AC3_3R	-63.3	89.5	28.3	-129.5	-103.7	29.8	145.4	91.1
	AC3_4	-87.8	97.3	31.8	-147.7	174.2	-50.1	59.7	91.3
	AC3_1	35.5	-102.3	31.8	-141.9	38.7	174.2	-71.2	-86.2
$[\text{G5'}\text{p-H}]^-$	AC3_3	-72.1	96.4	22.1	-124.8	-94.1	40.0	155.5	89.5

respectively. In this conformation, the excess negative charge on the phosphate group is solvated by two hydrogen bonding interactions, one with the C3' hydroxyl hydrogen atom of the ribose moiety and the other with the C2 amino hydrogen atom of guanine, and is designated as the SC3_1 conformer in Figure 7. This additional hydrogen bonding interaction between the phosphate and guanine moieties thus induces the change in the orientation of the nucleobase from *anti* to *syn*. Again, the 2'-hydroxyl hydrogen atom is oriented toward and aligned with the C3' hydroxyl oxygen atom to form a third hydrogen bond.

Stable low-energy conformers found for $[\text{A5'}\text{p-H}]^-$ and $[\text{U5'}\text{p-H}]^-$ are highly parallel to their DNA analogues. Virtually all stable low-energy conformers exhibit only the *anti* and C3' *endo* conformations, and the intramolecular hydrogen bonding interaction between one of the phosphate oxo oxygen atoms and the C3' hydroxyl oxygen atom, but differ from each other in the $\angle\text{OC5'}\text{C4'}\text{C3'}$ and $\angle\text{POC5'}\text{C4'}$ dihedral angles and the orientation of the free oxo oxygen atom and phosphate hydroxyl group. Only the AC3_5 conformer of $[\text{A5'}\text{p-H}]^-$ exhibits a different conformation of the ribose, where the

$\angle\text{C1'}\text{C2'}\text{C3'}\text{C4'}$ dihedral angle is -6.4° and the C3' atom lies in the plane of the ribose. Similar to the ground-state conformers described previously, the C2' hydroxyl hydrogen atom of these stable low-energy conformers also aligns with the C3' hydroxyl oxygen atom to form an additional hydrogen bonding interaction. In the case of $[\text{C5'}\text{p-H}]^-$, the ground-state and two of the stable low-energy conformers exhibit parallel behavior to that of $[\text{A5'}\text{p-H}]^-$ and $[\text{U5'}\text{p-H}]^-$. Several other stable low-energy conformers of $[\text{C5'}\text{p-H}]^-$ are found that either lack an intramolecular hydrogen bond between the C2' and C3' hydroxyl groups or exist in the C2' *endo* conformation where the C2' hydroxyl hydrogen atom forms an intramolecular hydrogen bond with the C2 carbonyl group of the nucleobase, and the C3' hydroxyl hydrogen atom is oriented toward the C2' hydroxyl oxygen atom to form a second intramolecular hydrogen bond. The stable low-energy conformers of $[\text{G5'}\text{p-H}]^-$ exhibit only the *syn* and C3' *endo* conformations, and the C3' hydroxyl hydrogen and C2 amino hydrogen atoms are hydrogen bonded to the phosphate oxo or hydroxyl oxygen atoms. Again, only the $\angle\text{OC5'}\text{C4'}\text{C3'}$ and

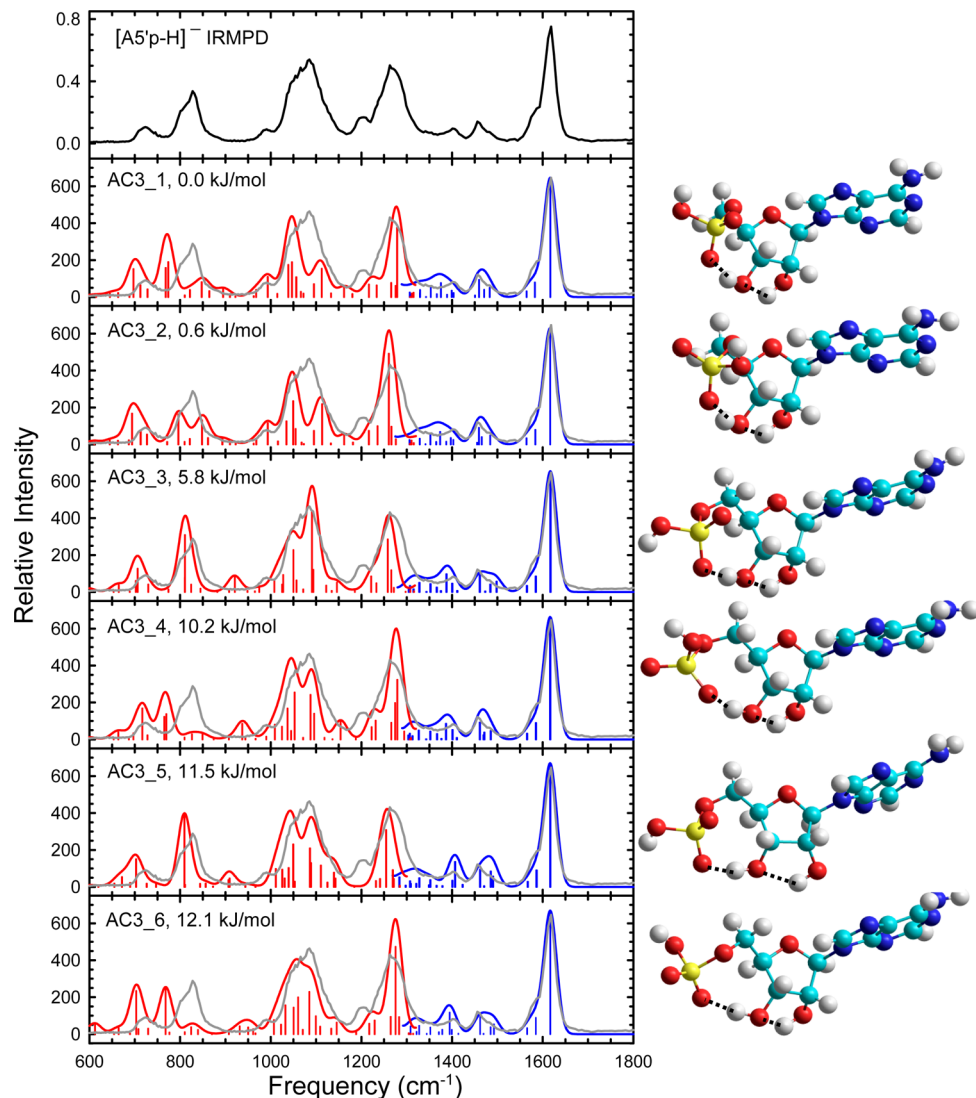


Figure 4. Comparison of the measured IRMPD action spectrum of $[A5'p\text{-H}]^-$ with the linear IR spectra and optimized structures predicted for the ground-state and stable low-energy conformers at the B3LYP/6-311+G(d,p) level of theory. Two scaling factors have been applied to the computed frequencies, 0.978 for frequencies above 1300 cm^{-1} (shown in blue in the computed spectra) and 1.00 for frequencies below 1300 cm^{-1} (shown in red in the computed spectra). To facilitate comparison of the measured and computed spectra, the IRMPD spectrum is overlaid with each of the computed spectra and scaled to match the intensity of the most intense feature. Relative Gibbs free energies at 298 K calculated at the MP2(full)/6-311+G(2d,2p) level of theory are also shown.

$\angle\text{POCS}'\text{C4}'$ dihedral angles and the orientations of the free oxo oxygen atom and phosphate hydroxyl group distinguish these low-energy conformers. A detailed discussion of the stable low-energy conformers of each of the deprotonated RNA mononucleotides is included in the Supporting Information.

Enthalpies and Gibbs free energies relative to the ground-state conformation calculated at the B3LYP, B3P86, M06, and MP2(full) levels of theory using the 6-311+G(2d,2p) basis set, including ZPE and thermal corrections at 298 K for all stable low-energy conformers computed of the four $[X5'p\text{-H}]^-$ ions, are summarized in Table 2 and compared in Figures S1–S4 of the Supporting Information. To simplify comparisons, Figures S1 and S2 (Supporting Information) do not include the P-OH rotamers. The relative enthalpies at 0 K, ΔH_0 values, determined for all four levels of theory are generally very consistent. Only in the case of $[A5'p\text{-H}]^-$ is there disagreement in the ground-state conformer where the B3LYP and B3P86 levels of theory suggests that the AC3_3 conformer is the

ground-state rather than the AC3_1 conformer, as found by both the MP2(full) and M06 levels of theory. In the case of $[C5'p\text{-H}]^-$ and $[U5'p\text{-H}]^-$, all four levels of theory find AC3_1 to be the ground-state conformer, whereas the SC3_1 conformer is the ground state of $[G5'p\text{-H}]^-$. Unlike the deprotonated DNA mononucleotides, the relative stabilities for the stable low-energy conformers of the RNA analogues studied here do not exhibit a consistent trend across all four levels of theory examined, as shown in Figure S1 (Supporting Information). Only for $[G5'p\text{-H}]^-$, where the relative enthalpy differences are less than 2.5 kJ/mol for all four levels of theory, is a consistent trend in stability found. However, consistent trends are found for all four deprotonated RNA mononucleotides by the B3LYP and B3P86 levels of theory, and separately by MP2(full) and M06, where the relative enthalpy differences lie within 2.4 and 6.8 kJ/mol, respectively. Because the ions are generated and probed at room temperature, thermal and entropy effects at 298 K may alter the relative stabilities of the

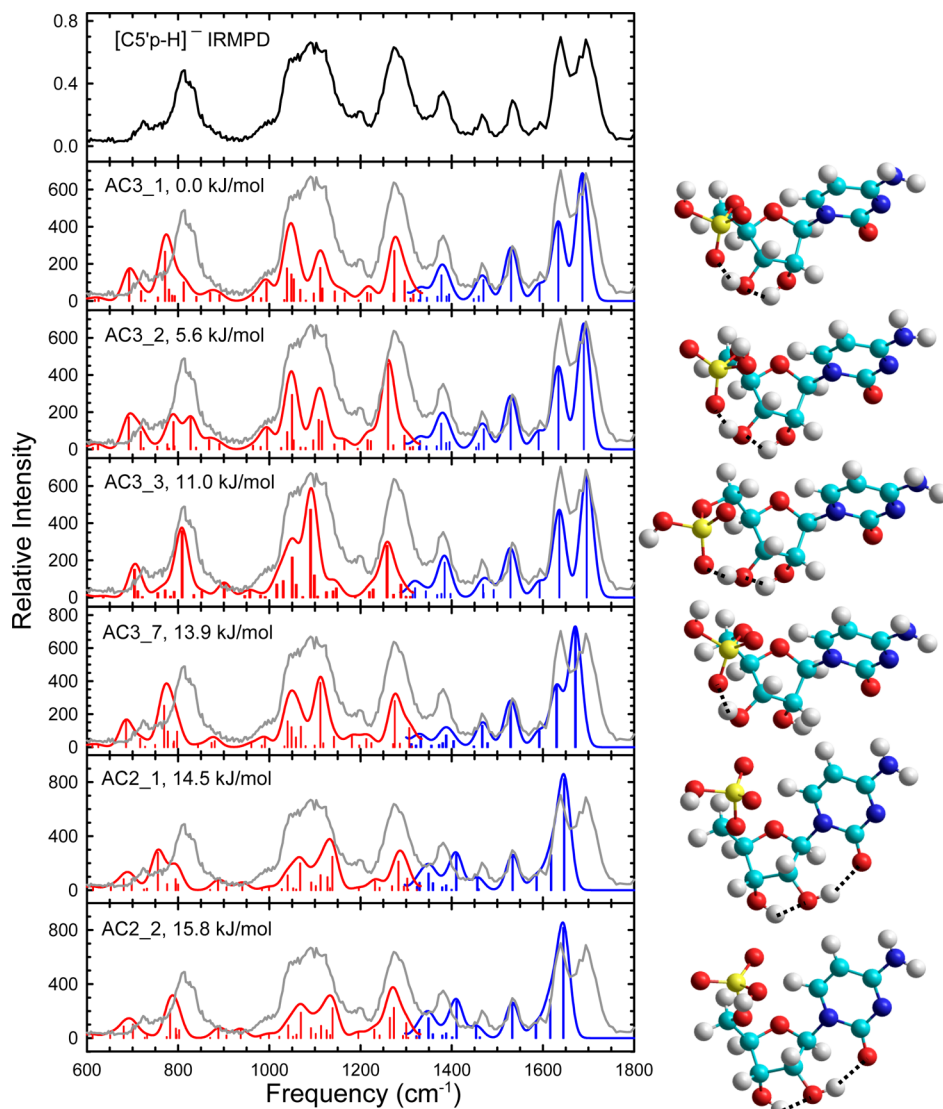


Figure 5. Comparison of the measured IRMPD action spectrum of $[C5'p-H]^-$ with the linear IR spectra and optimized structures predicted for the ground-state and stable low-energy conformers at the B3LYP/6-311+G(d,p) level of theory. Two scaling factors have been applied to the computed frequencies, 0.978 for frequencies above 1300 cm^{-1} (shown in blue in the computed spectra) and 1.00 for frequencies below 1300 cm^{-1} (shown in red in the computed spectra). To facilitate comparison of the measured and computed spectra, the IRMPD spectrum is overlaid with each of the computed spectra and scaled to match the intensity of the most intense feature. Relative Gibbs free energies at 298 K calculated at the MP2(full)/6-311+G(2d,2p) level of theory are also shown.

stable low-energy conformers of the deprotonated RNA mononucleotides, and are therefore included in Table 2 and Figures S2 and S4 of the Supporting Information as relative 298 K Gibbs free energies (ΔG_{298}). The AC3_1 conformer remains the ground-state conformer for $[A5'p-H]^-$, $[C5'p-H]^-$, and $[U5'p-H]^-$, calculated at the MP2(full) and M06 levels of theory. The relative 298 K Gibbs free energies calculated using B3LYP and B3P86 theories provide the same result for $[C5'p-H]^-$, and the AC3_1 conformer remains the ground state. However, B3LYP and B3P86 find the AC3_3 conformer to be the ground state for $[A5'p-H]^-$, while a P-OH rotamer of the AC3_3 conformer, designated as AC3_3R shown in Figure S5 (Supporting Information), was calculated to be the ground-state conformer for $[U5'p-H]^-$. Only in the case of $[G5'p-H]^-$ do all four levels of theory agree that the SC3_1 conformer is the ground state. Trends in the relative 298 K Gibbs free energies of the stable low-energy conformers are highly parallel to the relative 0 K enthalpies. The largest deviation observed

between B3LYP and B3P86 is 2.4 kJ/mol, while the MP2(full) and M06 energies lie within 6.8 kJ/mol. Overall, the MP2(full) and M06 levels of theory provide the most consistent trends for the ground-state and low-energy conformers of each deprotonated RNA mononucleotide, and because the MP2(full) level of theory generally provides the most reliable energetic information among the theories employed here,^{20,45,51} the Gibbs free energies calculated at the MP2(full)/6-311+G(2d,2p) level of theory will be used throughout the remaining discussion, while the optimized structures and theoretical linear IR spectra are calculated at the B3LYP/6-311+G(d,p) level of theory.

Comparison of Experimental and Theoretical IR Spectra of $[X5'p-H]^-$. Structures of all stable low-energy conformers of the four deprotonated RNA mononucleotides, $[X5'p-H]^-$, within 15 kJ/mol of the ground-state conformation calculated at the B3LYP/6-311+G(2d,2p) level of theory and their MP2(full)/6-311+G(2d,2p) relative Gibbs free energies at

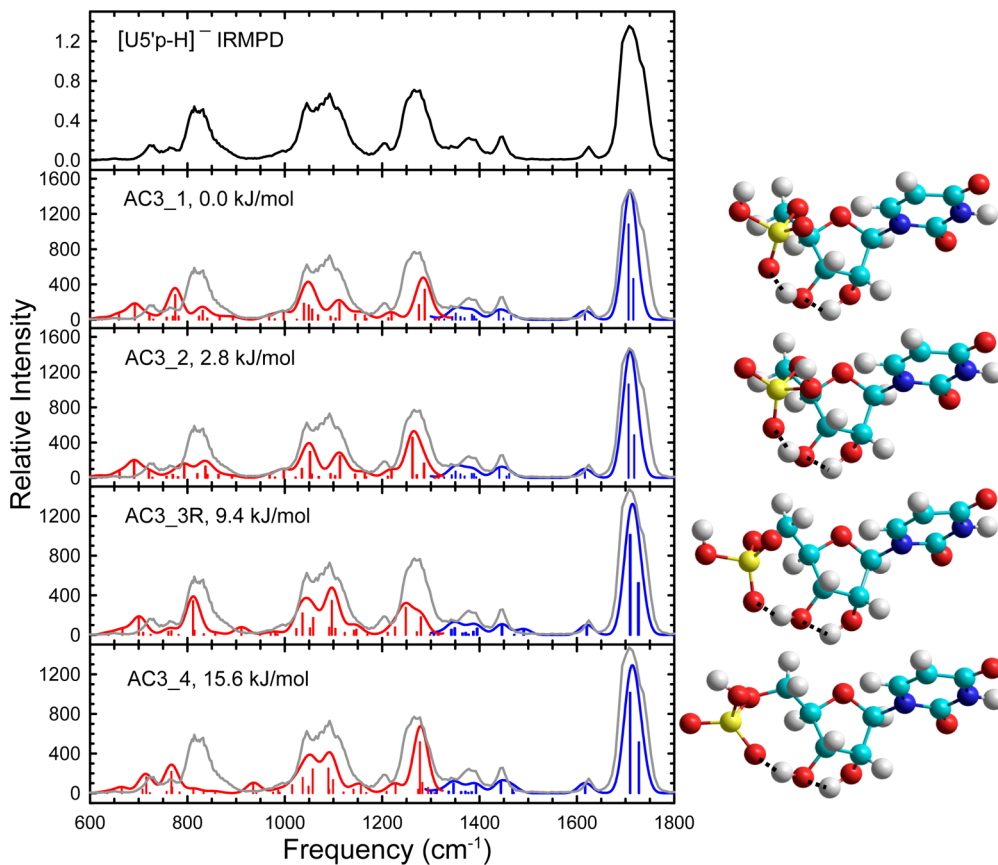


Figure 6. Comparison of the measured IRMPD action spectrum of $[U5'p-H]^-$ with the linear IR spectra and optimized structures predicted for the ground-state and stable low-energy conformers at the B3LYP/6-311+G(d,p) level of theory. Two scaling factors have been applied to the computed frequencies, 0.978 for frequencies above 1300 cm^{-1} (shown in blue in the computed spectra) and 1.00 for frequencies below 1300 cm^{-1} (shown in red in the computed spectra). To facilitate comparison of the measured and computed spectra, the IRMPD spectrum is overlaid with each of the computed spectra and scaled to match the intensity of the most intense feature. Relative Gibbs free energies at 298 K calculated at the MP2(full)/6-311+G(2d,2p) level of theory are also shown.

298 K are shown in Figures 4–7 along with their calculated linear IR spectra. Hydroxyl rotamers of the phosphate group that cannot be differentiated by their calculated linear IR spectra are not included in these figures. All stable low-energy conformers of these species and their relative 298 K Gibbs free energies are compared in Figure S5 of the Supporting Information. Also shown in these figures are the experimental IRMPD action spectra of the four deprotonated RNA mononucleotides. To facilitate these comparisons, the measured IRMPD spectra are overlaid with each of the computed IR spectra and scaled to match the intensity of the most intense feature. In all cases, the assignment of the stable conformer(s) accessed in the experiments is based primarily on the agreement between the measured and computed band positions (vibrational frequencies), and secondarily on the relative energetics computed by theory.

Similar to that found for the deprotonated DNA mononucleotides, the spectral features in the region extending from ~ 1300 to 1650 cm^{-1} are sufficiently similar for all stable low-energy conformers of each deprotonated mononucleotide that adopts a given conformation of the nucleobase moiety (either *anti* or *syn*), and thus cannot be used effectively to identify the presence of different conformers in the experiments. The spectral similarities among the low-energy conformers in this region are not surprising, as these features primarily arise from the stretching modes of the nucleobase,

and the conformation of the nucleobase remains virtually unchanged across the low-energy conformers of each of the deprotonated RNA mononucleotides. In contrast, the calculated linear IR spectra of the deprotonated RNA mononucleotides in the spectral region from ~ 700 to 1300 cm^{-1} are more characteristic of each conformer, and thus are used to determine which conformers are accessed in the experiments. However, the measured IRMPD spectra in this region exhibit severely broadened features due to the multiple photon nature of the technique, anharmonicity of the phosphate-oxygen stretching modes, and the room temperature internal energy distribution of the ions, such that the theoretical IR spectra of multiple conformers of each deprotonated RNA mononucleotide exhibit good agreement. Thus, multiple conformers of each deprotonated RNA mononucleotide are likely accessed in the experiments. Indeed, the subtle differences in the IR and IRMPD spectra make it challenging to definitively rule out the presence of many of the low-energy conformers without consideration of their computed relative stabilities.

Comparison of Experimental and Theoretical IR Spectra of $[A5'p-H]^-$. The experimental IRMPD action spectrum and the calculated linear IR spectra of $[A5'p-H]^-$ and their optimized structures are compared in Figure 4. The calculated IR spectrum of the AC3_1 conformer exhibits good agreement with the measured IRMPD action spectrum for most of the major bands predicted by theory. However, the

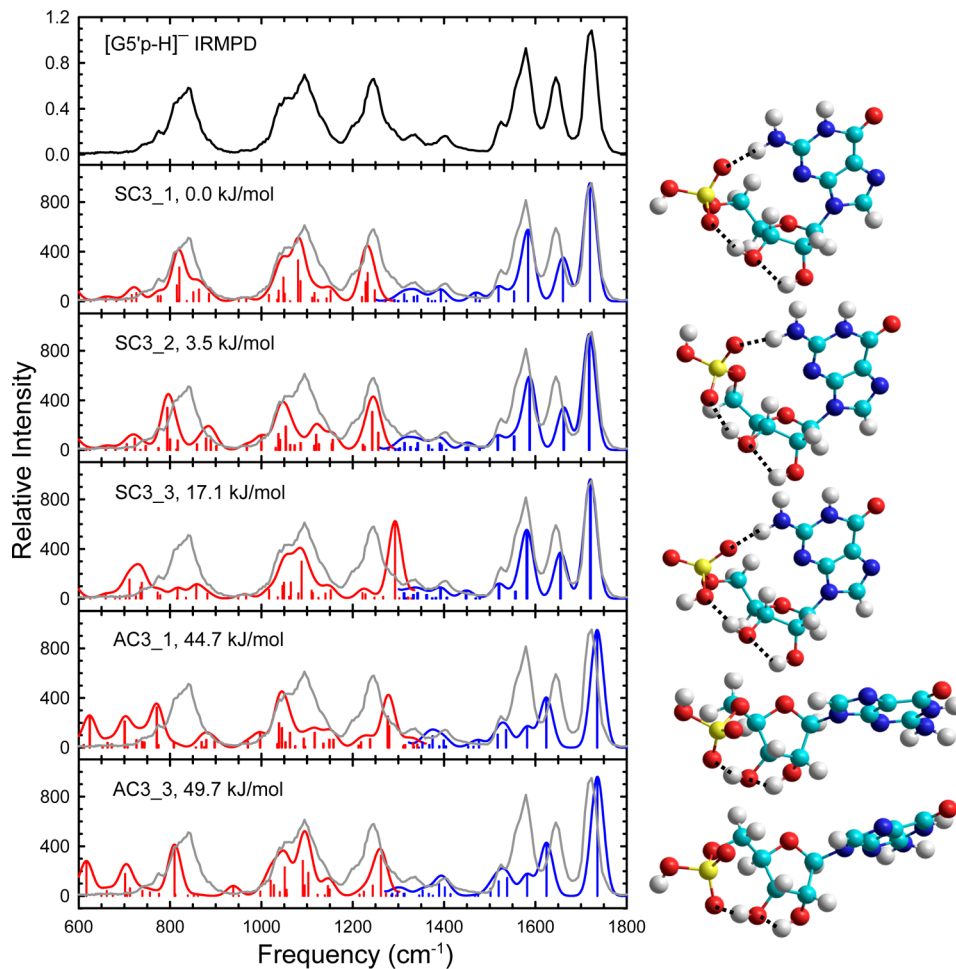


Figure 7. Comparison of the measured IRMPD action spectrum of $[G5'p\text{-H}]^-$ with the linear IR spectra and optimized structures predicted for the ground-state and stable low-energy conformers at the B3LYP/6-311+G(d,p) level of theory. Two scaling factors have been applied to the computed frequencies, 0.978 for frequencies above 1300 cm^{-1} (shown in blue in the computed spectra) and 1.00 for frequencies below 1300 cm^{-1} (shown in red in the computed spectra). To facilitate comparison of the measured and computed spectra, the IRMPD spectrum is overlaid with each of the computed spectra and scaled to match the intensity of the most intense feature. Relative Gibbs free energies at 298 K calculated at the MP2(full)/6-311+G(2d,2p) level of theory are also shown.

broad band centered at $\sim 825\text{ cm}^{-1}$ in the IRMPD spectrum is red-shifted by $\sim 50\text{ cm}^{-1}$ in the computed spectrum. Other differences between the IRMPD and AC3_1 spectra include red shifting by 25 cm^{-1} of the two minor bands observed at 700 and 1375 cm^{-1} and blue shifting by 25 cm^{-1} of the band observed at 1225 cm^{-1} in the calculated spectrum. The predicted spectrum of the AC3_2 conformer is similar to that of the AC3_1 conformer, and also displays a good match to the measured spectrum. However, two major differences between the AC3_2 spectrum and experimental spectrum are observed. The broad band at $\sim 825\text{ cm}^{-1}$ in the IRMPD action spectrum is split into two bands, and the blue shifting of the minor features near 1200 cm^{-1} lead to a tail rather than a resolved feature to the red of the intense band at $\sim 1260\text{ cm}^{-1}$ of the theoretical spectrum. The broad band at around 825 cm^{-1} in the IRMPD action spectrum seems to arise from two closely spaced IR active modes because the band is asymmetric, with a sharp feature at $\sim 825\text{ cm}^{-1}$ and a shoulder to the red at $\sim 800\text{ cm}^{-1}$. Comparison of this feature to the theoretical spectra suggests that the peaks at 775 and 850 cm^{-1} of the AC3_1 spectrum and the peaks at 800 and 850 cm^{-1} of the AC3_2 spectrum are underestimated by the B3LYP level of theory and should be blue-shifted and red-shifted, respectively, to produce

the broad asymmetric IRMPD feature. Comparison of the IRMPD action spectrum to the calculated linear IR spectrum for the AC3_3 conformer also exhibits good agreement for the major bands at 1080 , 1275 , and 1620 cm^{-1} of the measured spectrum, while the bands at 705 and 810 cm^{-1} of the theoretical spectrum are red-shifted by 20 and 15 cm^{-1} , respectively. However, the absence of the band computed at 920 cm^{-1} in the measured IRMPD spectrum, suggests that this low-energy conformer is not a major contributor in the experiments. A similar comparison can also be made with the theoretical spectrum calculated for the AC3_4 conformer. However, the presence of an additional peak at 1150 cm^{-1} and the red-shifted band at 770 cm^{-1} of the theoretical spectrum suggest that the AC3_4 conformer, which is relatively high in free energy as compared to the ground-state conformer (10.2 kJ/mol), is most likely not an important contributor in the experiments. The calculated linear IR spectrum of the AC3_5 conformer displays many spectral features that closely resemble the AC3_3 spectrum. This is not surprising, considering that the greatest difference between the AC3_3 and AC3_5 conformers is the puckering of the ribose moiety, shown in Table 1, and is probably best illustrated by the spectral features extending from 980 to 1175 cm^{-1} in their theoretical spectra.

Table 2. Relative Enthalpies at 0 K and Gibbs Free Energies at 298 K of the Stable Low-Energy Conformers and Select Excited Conformers of the Deprotonated RNA Mononucleotides Calculated at Various Levels of Theory^a

complex	conformer	MP2(full)		M06		B3LYP		B3P86	
		ΔH_0	ΔG_{298}						
[A5'p-H] ⁻	AC3_1	0.0	0.0	0.0	0.0	0.6	4.0	0.3	3.7
	AC3_2	2.9	0.6	3.0	0.6	3.8	4.8	3.7	4.7
	AC3_1R	3.7	3.0	3.4	2.8	4.3	7.0	3.8	6.5
	AC3_3	9.1	5.8	4.8	1.4	0.0	0.0	0.0	0.0
	AC3_2R	7.8	7.9	7.0	7.1	7.4	10.9	7.0	10.5
	AC3_3R	12.0	8.5	7.0	3.5	0.9	0.7	1.4	1.2
	AC3_4	13.7	10.2	8.0	4.5	1.6	1.5	2.8	2.6
	AC3_5	15.3	11.5	11.9	8.1	2.0	1.6	1.9	1.5
	AC3_6	16.1	12.1	11.6	7.6	7.0	6.3	6.4	5.7
	AC3_4R	17.8	13.4	12.0	7.6	6.0	4.9	6.9	5.8
	AC3_5R	16.6	13.5	13.4	10.3	3.4	3.7	3.5	3.8
	AC3_6R	19.2	15.5	14.2	10.5	10.4	10.0	9.5	9.1
	SC3_1	22.9	19.9	19.8	16.8	10.7	11.1	11.8	12.1
	SC3_2	25.3	24.5	24.0	23.1	19.8	22.3	20.4	22.9
[C5'p-H] ⁻	AC3_1	0.0	0.0	0.0	0.0	0.0	0.0	0.0	0.0
	AC3_1R	2.5	1.5	2.4	1.4	2.8	1.7	2.5	1.5
	AC3_2	8.3	5.6	7.2	4.6	6.0	3.3	6.4	3.7
	AC3_2R	10.8	9.0	9.7	7.9	8.7	6.9	8.8	7.0
	AC3_3	15.8	11.0	10.7	5.8	5.6	0.8	6.3	1.5
	AC3_3R	19.8	13.8	14.1	8.2	7.4	1.4	8.5	2.5
	AC3_7	13.9	13.9	12.5	12.5	13.5	13.6	14.5	14.5
	AC2_1	14.6	14.5	11.8	11.7	10.5	10.5	12.2	12.1
	AC3_7R	15.9	15.1	14.3	13.6	15.9	15.1	16.5	15.8
	AC2_2	17.3	15.8	14.2	12.7	12.8	11.3	14.7	13.2
	SC3_1	48.9	43.9	44.5	39.5	30.9	25.9	33.9	28.8
	SC3_2	56.4	54.0	52.3	49.9	43.3	40.9	45.6	43.1
[U5'p-H] ⁻	AC3_1	0.0	0.0	0.0	0.0	0.0	2.5	0.0	1.8
	AC3_1R	3.5	2.6	3.4	2.5	3.6	5.2	3.3	4.3
	AC3_2	5.3	2.8	4.4	2.0	4.0	4.1	4.4	3.7
	AC3_3R	16.3	9.4	11.5	4.6	4.4	0.0	5.1	0.0
	AC3_2R	10.0	10.0	8.9	8.8	8.2	10.5	8.1	9.9
	AC3_3	12.9	10.0	8.9	6.1	3.9	3.5	3.8	2.8
	AC3_4	19.2	15.6	12.4	8.8	6.4	5.2	8.1	6.3
	SC3_1	36.7	33.5	32.2	29.0	21.2	20.4	23.5	22.0
	SC3_2	41.9	40.5	38.3	36.9	31.5	32.5	33.2	33.6
[G5'p-H] ⁻	SC3_1	0.0	0.0	0.0	0.0	0.0	0.0	0.0	0.0
	SC3_1R	1.8	2.0	2.0	2.2	2.0	2.2	2.0	2.2
	SC3_2	3.5	3.5	4.0	4.0	3.6	3.5	4.4	4.4
	SC3_2R	5.6	5.2	5.6	5.2	5.5	5.1	6.1	5.6
	SC3_3	19.0	17.1	19.6	17.8	18.6	16.8	21.0	19.2
	AC3_1	55.9	44.7	57.1	45.9	46.9	35.7	50.5	39.3
	AC3_3	62.6	49.7	60.7	47.8	43.9	31.0	47.8	34.9

^aEnergetics are determined from single-point energy calculations using the 6-311+G(2d,2p) basis set and structures optimized at the B3LYP/6-311+G(d,p) level of theory including zero-point vibrational energy and thermal corrections. All energies are given in kJ/mol.

The IR features in this region for the AC3_5 conformer are broadened as compared to those of the AC3_3 conformer. However, the absence of the minor feature at 1200 cm⁻¹, the narrowing of the feature at ~1255 cm⁻¹, and the red shifting of the feature calculated at 1040 cm⁻¹ provide the best evidence for suggesting that this conformer is not accessed in significant abundance in the experiments. Similar to previous comparisons, good agreement with the measured IRMPD spectrum is also found for several of the major peaks in the calculated IR spectrum of the AC3_6 conformer. However, the presence of an absorption band at ~950 cm⁻¹ in the theoretical spectrum, but clearly absent in the measured spectrum, the red shifting of the features calculated at ~700, 760, and 1050 cm⁻¹ as

compared to the IRMPD spectrum, and the relatively high free energy as compared to the ground-state AC3_1 conformer, 12.1 kJ/mol, suggest that the AC3_6 conformer is also not a dominant contributor to the experimental spectrum. However, without consideration of the computed energetics, the modest differences in the IRMPD and calculated IR spectra for all six low-energy conformers, it is impossible to definitively rule out a small population of any of these species in the experiments.

Comparison of Experimental and Theoretical IR Spectra of [C5'p-H]⁻. The experimental IRMPD action spectrum and the calculated linear IR spectra of [C5'p-H]⁻ and their optimized structures are compared in Figure 5. The theoretical spectrum of the ground-state AC3_1 conformer

reproduces the measured IRMPD action spectrum very well, except for the slightly broad and asymmetric feature at $\sim 815 \text{ cm}^{-1}$ of the experimental spectrum that is again red-shifted by $\sim 50 \text{ cm}^{-1}$ in the AC3_1 spectrum. This consistent difference in the measured and calculated spectra suggests that the B3LYP level of theory is underestimating the IR frequencies in this spectral region. Likewise, the weak band observed just to the red at $\sim 725 \text{ cm}^{-1}$ also appears to be red-shifted by 25 cm^{-1} in the calculated spectrum, while the minor band observed at $\sim 1200 \text{ cm}^{-1}$ is blue-shifted by 25 cm^{-1} . Aside from the modest shift in the intensities or band positions in the spectral region extending from 750 to 850 cm^{-1} and 1200 to 1300 cm^{-1} , the predicted spectrum for the AC3_2 conformer is remarkably similar to that of the AC3_1 conformer. In addition, it agrees well with the IRMPD action spectrum, thus suggesting that this conformer may also be an important contributor to the measured spectrum. Comparison of the theoretical IR spectrum of the AC3_3 conformer to the IRMPD action spectrum also exhibits good agreement due to the significant broadening of several major peaks in the experimental spectrum, as well as the lack of variation in the nucleobase stretching region. However, the large decrease in intensity and the red shifting of the feature observed at 1275 cm^{-1} and the relatively high Gibbs free energy as compared to the ground-state conformer are probably most diagnostic for concluding that the AC3_3 is probably only a modest contributor to the measured spectrum. Unlike the ground-state and the first two excited low-energy conformers, the bands in the nucleobase stretching region for the theoretical spectra of the AC3_7, AC2_1, and AC2_2 conformers are sufficiently different from the IRMPD action spectrum that these conformers can be ruled out as possible contributors to the experimental spectrum. The changes to the nucleobase stretching bands for the AC2_1 and AC2_2 conformers are most likely due to the intramolecular hydrogen bond formed between the C2' hydroxyl group of the ribose moiety and the C2 carbonyl group of the nucleobase that weakens the C=O bond, thus red shifting the carbonyl stretch to 1645 cm^{-1} , while other nucleobase stretching modes are also slightly affected. The unperturbed carbonyl stretch for the ground-state and first two excited conformers arises at 1690 cm^{-1} of the theoretical spectra. The carbonyl stretching mode in the calculated spectrum of the AC3_7 conformer is also red-shifted by $\sim 15 \text{ cm}^{-1}$ as compared to the AC3_1 spectrum, even though these two structures only differ by the orientation of the 2'-hydroxyl hydrogen atom. The distance between the 2'-hydroxyl hydrogen atom and the carbonyl oxygen atom is 3.4 \AA , such that the hydrogen bonding interaction is very weak and only a modest shift in the carbonyl stretch is computed. It should be noted here that the theoretical IR spectra of the AC3_1 and AC3_7 conformers exhibit several small differences in the region extending from 650 to 1300 cm^{-1} that possibly arise from the different orientations of the 2'-hydroxyl group. However, due to the severe broadening of the bands observed in this region in the measured spectrum, it would be very challenging to distinguish the two conformers if the nucleobase stretching region did not contain diagnostic bands.

Comparison of Experimental and Theoretical IR Spectra of [U5'p-H]⁻. The experimental IRMPD action spectrum and the calculated linear IR spectra of [U5'p-H]⁻ and their optimized structures are compared in Figure 6. The predicted bands from 830 to 1325 cm^{-1} for the AC3_1 and AC3_2 conformers are reasonably well matched to the IRMPD action spectrum of [U5'p-H]⁻, whereas a blue shift of the

bands at 775 and 795 cm^{-1} of the AC3_1 and AC3_2 spectra, respectively, as well as the bands at 690 cm^{-1} for both conformers is necessary to achieve agreement with the experimental spectrum. Nonetheless, the ground-state AC3_1 and the first-excited AC3_2 conformers are most likely the dominant structures accessed in the experiments, as these bands are largely due to the phosphate moiety and were also underestimated in the spectra of [AS'p-H]⁻. The AC3_3R conformer also exhibits good agreement with the measured IRMPD spectrum, except that the intensities of the major bands observed at ~ 870 and 1275 cm^{-1} are more red-shifted and suppressed even more than found for the AC3_1 and AC3_2 conformers. However, these differences are insufficient to rule out this conformer in the experiments, but the higher relative Gibbs free energy of this conformer suggests that it is probably a less important contributor than the AC3_1 and AC3_2 conformers. Similarly, the absence of the broad band observed at $\sim 820 \text{ cm}^{-1}$ and the appearance of the minor band at 940 cm^{-1} in the computed spectrum for the AC3_4 conformer, but absent in the measured spectrum, as well as its relatively high free energy as compared to the ground-state AC3_1 conformer (15.6 kJ/mol), suggest that this conformer does not contribute significantly to the experiments.

Comparison of Experimental and Theoretical IR Spectra of [G5'p-H]⁻. The experimental IRMPD action spectrum and the calculated linear IR spectra of [G5'p-H]⁻ and their optimized structures are compared in Figure 7. In the overall comparison, the IRMPD action spectrum of [G5'p-H]⁻ is clearly best reproduced by the theoretical spectrum of the SC3_1 conformer, suggesting that the ground-state conformer is the dominant species accessed in the experiments. However, the bands observed at 740 , 1100 , and 1250 cm^{-1} are red-shifted by 20 cm^{-1} , and the band observed at 1650 cm^{-1} is blue-shifted by 10 cm^{-1} , again indicating that theory has trouble describing the phosphate stretches. In comparison, the calculated spectrum for the SC3_2 conformer exhibits somewhat poorer agreement with the experimental spectrum. In particular, the shapes of the bands in the 750 – 900 and 950 – 1200 cm^{-1} regions are not well reproduced in the computed spectrum. However, these computed features still almost fit under the envelopes of these broad features, and the relatively small difference in the Gibbs free energy as compared to the ground-state SC3_1 conformer suggests that a small population of the SC3_2 conformer may still be accessed in the experiments. The SC3_3 conformer, which is calculated to be 17.1 kJ/mol less stable than the SC3_1 conformer, appears to be unimportant due to the appearance of the moderately intense broad band at 730 cm^{-1} and the sharp peak at 1300 cm^{-1} of the SC3_3 conformer, which is not observed in the IRMPD action spectrum. The linear IR spectra of the analogous *anti* conformations, AC3_3 and AC3_1, are also included in Figure 7 in an attempt to confirm that the *syn* and *anti* conformers can indeed be differentiated by their IR spectra. As can be seen in the figures, the *anti* and *syn* conformers of [G5'p-H]⁻ exhibit significant differences in the spectral regions 600 – 850 and 1300 – 1800 cm^{-1} , the regions associated with the bending and stretching modes of the nucleobase. Thus, these high Gibbs free energy *anti* conformers, AC3_1 and AC3_3, can be ruled out as contributors to the measured IRMPD spectrum.

***syn* and *anti* Differentiation in the Absence of Hydrogen Bonding.** The *syn* analogues of the AC3_1 and AC3_3 conformers for [AS'p-H]⁻, [C5'p-H]⁻, and [U5'p-H]⁻, the SC3_2 and SC3_1 conformers, were also optimized and

their theoretical spectra calculated to again determine whether or not the *syn* and *anti* conformers can be differentiated by their IR spectra, and are included in Figures S5–S8 of the Supporting Information. These *syn* conformers differ from the ground-state and first-excited low-energy conformers of $[G5'p-H]^-$ in that the nucleobase and phosphate moiety do not form a hydrogen bonding interaction, and as a result are oriented further away from each other, as shown by the $\angle N9C1'C4'$ angle for $[A5'p-H]^-$ and $[G5'p-H]^-$, the $\angle N1C1'C4'$ angle for $[C5'p-H]^-$ and $[U5'p-H]^-$ of the ribose and nucleobase moieties, and the $\angle OC5'C4'C3'$ dihedral angle in Table S3 of the Supporting Information. In addition, the nucleobase moieties of these *syn* conformers do not sit directly above the plane of the ribose as in the case of $[G5'p-H]^-$. Instead, the nucleobases are oriented slightly away from the plane of the ribose moiety, as shown by the difference in the $\angle OC1'N9C4$ dihedral angles of $[A5'p-H]^-$ and $[G5'p-H]^-$, and $\angle OC1'N1C2$ dihedral angles of $[C5'p-H]^-$ and $[U5'p-H]^-$. Surprisingly, the IR features in the nucleobase bending and stretching regions of the *anti* and *syn* conformers for $[A5'p-H]^-$, between 600–850 and 1300–1800 cm^{-1} , do not exhibit sufficient variation to allow the differentiation of these conformers. Instead, the small band at $\sim 940 \text{ cm}^{-1}$, the partially resolved broad band that extends from 990 to 1170 cm^{-1} for the SC3_1 conformer, and the small bands at 765 and 890 cm^{-1} of the SC3_2 conformer provide the best indications that these two relatively high-energy conformers are not accessed in the experiments. In the case of $[C5'p-H]^-$ and $[U5'p-H]^-$, the predicted spectra for the SC3_1 and SC3_2 conformers exhibit apparent variation from the AC3_1 and AC3_3 conformers in the nucleobase stretching region that spans from 1300 to 1800 cm^{-1} , shown in Figures S7 and S8 (Supporting Information), but not in the region 600–850 cm^{-1} . Nonetheless, based on comparison of the IRMPD action spectrum and the theoretical spectra of SC3_1 and SC3_2 conformers for both $[C5'p-H]^-$ and $[U5'p-H]^-$, the presence of these conformers, which are computed to be relatively high in free energy, can be ruled out.

Vibrational Assignments. Vibrational assignments of the features observed in the experimental IRMPD action spectra of the deprotonated RNA mononucleotides are summarized in Tables S1 and S2 of the Supporting Information and are based on comparisons to the theoretical IR spectra computed for the stable low-energy conformers that are most likely accessed in the experiments. Thus, the vibrational assignments are based on the AC3_1, AC3_2, and AC3_3 conformers of $[A5'p-H]^-$, $[C5'p-H]^-$, and $[U5'p-H]^-$ and the SC3_1 and SC3_2 conformers of $[G5'p-H]^-$. Band positions for the AC3_1 and AC3_3 conformers of $[G5'p-H]^-$ are also included in Tables S1 and S2 (Supporting Information) for comparison. Modes that rule out the presence of the *anti* conformers of $[G5'p-H]^-$ in the experiments are italicized. As inferred above from comparison of the IRMPD spectra of the four deprotonated RNA mononucleotides and that of $[DEP-H]^-$, the bands from 700 to 1300 cm^{-1} arise primarily from the vibrational modes of the phosphate and ribose moieties with minor contributions from mixed character modes associated with the nucleobase, whereas the bands in the region from ~ 1300 to 1800 cm^{-1} are primarily due to the IR active modes of the nucleobase with minor contributions from mixed character modes of the ribose moiety.

Comparison to Deiprotonated DNA Mononucleotides. The IRMPD action spectra of the deprotonated RNA mononucleotides are compared to those measured previously

for the analogous deprotonated DNA mononucleotides in Figure 8.⁴⁰ Although the IRMPD action spectra for the

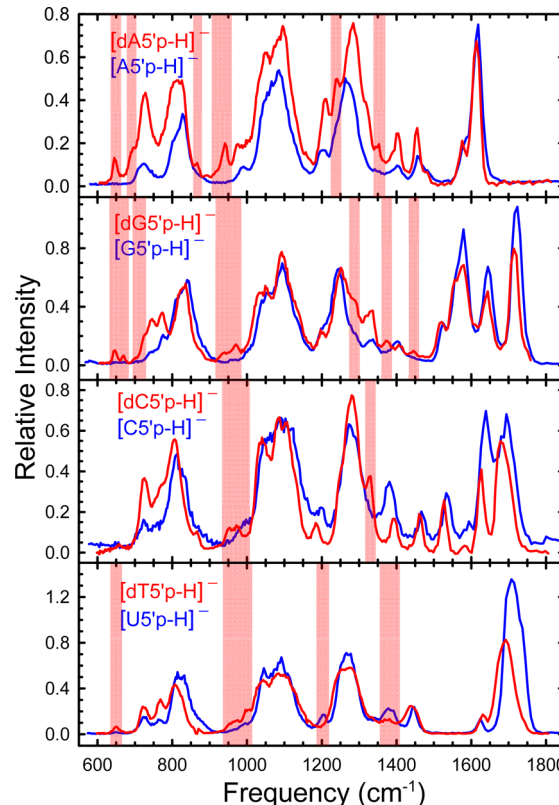


Figure 8. Comparison of the measured IRMPD action spectra of $[dX5'p-H]^-$ and $[X5'p-H]^-$. Major differences between the analogous spectra are highlighted. Results for $[dX5'p-H]^-$ are taken from ref 40.

deprotonated DNA and RNA mononucleotides are remarkably similar, minor differences are observed and highlighted in the figure. These small differences are not only found in the IR active regions of the phosphate and ribose moieties, 650–1400 cm^{-1} , but also in the nucleobase vibrational region, suggesting that the 2'-hydroxyl group exerts more profound effects than simply enhancing the intensities of the C–O and O–H bending and stretching modes; i.e., shifting and/or coupling of the vibrational bands of the phosphate and nucleobase moieties are clearly impacted. In general, the IRMPD yield of the deprotonated RNA mononucleotides is slightly lower than the yield for the deprotonated DNA mononucleotides, except in the case of $[dA5'p-H]^-$ versus $[A5'p-H]^-$, where larger differences are observed. The reduction in the IRMPD yield suggests that the 2'-hydroxyl most likely reduces the yield by increasing the barrier for the activated dissociation rather than affecting the IVR efficiency, consistent with the nucleobase anions being observed for the deprotonated DNA but not the RNA mononucleotides.

Comparison of the ground-state and stable low-energy conformers found here for the deprotonated RNA mononucleotides to the structures reported previously for the deprotonated DNA mononucleotides suggests that the 2'-hydroxyl group does not exert a major influence on the overall structure of the mononucleotides, as the ground-state and stable low-energy conformers of $[X5'p-H]^-$ are highly parallel to those of $[dX5'p-H]^-$. The 2'-hydroxyl group does however provide additional stabilization to the overall structure via a

hydrogen bonding interaction between the 2'-hydroxyl hydrogen and 3'-hydroxyl oxygen atoms, respectively. Only in the case of $[CS'p-H]^-$ is the C2' *endo* conformation found among the stable low-energy conformers, AC2_1 and AC2_2. In both the deprotonated DNA and RNA mononucleotides, comparisons of the measured IRMPD action spectra to the calculated linear IR spectra suggest that multiple conformers were accessed in the experiments. However, in the case of the deprotonated RNA mononucleotides, fewer conformers were accessed in the experiments, as limited by their ability to form the intramolecular hydrogen bond between the C2' and C3' hydroxyl groups. Nonetheless, the highly parallel results in the conformations of the deprotonated DNA and RNA mononucleotides suggest that the fundamental difference in the biological roles and functions of the DNA and RNA monomers is most likely not due to their relative conformations, and thus is more likely related to their differences in chemical properties. Whether or not this conclusion remains true in the presence of protons and sodium cations is currently under investigation and will be the subject of a series of studies to follow.

Comparison to Other Experimental Techniques. de Vries and co-workers previously examined the neutral forms of 9-ethyl guanine, guanosine, and 2'-deoxyguanosine in the mid-IR region, 500–2000 cm^{-1} , using UV-IR double resonance techniques and theoretical calculations.¹⁷ The most stable conformer calculated for guanosine in their study using the RI-MP2/cc-pVDZ level of theory exhibits the C2' *endo* conformation for the ribose and the *syn* conformation for the nucleobase, and the N3 nitrogen atom of the nucleobase forms a hydrogen bonding interaction with the 5'-hydroxyl hydrogen atom. This differs from the ribose conformation observed in the current study, the C3' *endo* conformation, for guanosine-5'-monophosphate and may suggest that the deprotonated phosphate moiety induces this change in the sugar conformation. The enol-imino (O6–N1) tautomer is also considered in their calculations, and is found to be 3.1 kJ/mol less stable than the canonical keto-amino tautomer. Comparison of the IR-UV ion-dip spectrum of guanosine to the theoretical IR spectra calculated using both the RI-MP2/cc-pVDZ and RI-DFT-D (TSSP) levels of theory suggests that the enol-imino tautomer was accessed in their experiment due to the absence of a sharp carbonyl stretch at ~ 1700 – 1725 cm^{-1} . This is markedly different from the results observed in the current study in which a strong carbonyl stretch is present in the IRMPD action spectrum of $[G5'p-H]^-$ at $\sim 1735 \text{ cm}^{-1}$, indicating that the ground-state canonical keto-amino tautomer of the nucleotide was accessed in our experiments. It is possible that the difference in the conformation of the nucleobase accessed in our experiments and that of de Vries and co-workers is due to the presence of the deprotonated phosphate moiety and the additional hydrogen bond stabilization with the N2 amino group of the nucleobase moiety. However, it seems more likely that the slightly higher energy enol-imino tautomer accessed in the work of de Vries and co-workers is due to the difference in the way in which these species were introduced into the gas phase. The neutral of interest was introduced into the gas phase via laser desorption in the IR-UV experiment, while electrospray ionization was employed here for the deprotonated species. In principle, the vibrational modes of the ribose from the IR-UV experiments can be used to compare to the modes observed in the current study in an attempt to assign different conformations of the ribose, C2' *endo* versus C3' *endo*. However, the vibrational

modes below 1350 cm^{-1} in the IRMPD action spectrum are significantly broadened as compared to the IR-UV ion-dip spectrum, and the coupling of ribose, phosphate, and nucleobase vibrational modes makes such a comparison very difficult. Therefore, such comparisons were not pursued, as they would probably not yield very useful information.

Leulliot et al. previously examined the aqueous and neutral forms of cytidine and uridine using FTIR and theoretical calculations, respectively, in the region below 2000 cm^{-1} .^{52,53} The ground-state conformers they calculated for both cytidine and uridine exhibit a C3' *endo* conformation for the ribose and *anti* conformation for the nucleobase, and the 2'-hydroxyl hydrogen atom forms an intramolecular bond with the oxygen atom of the C3' hydroxyl group, similar to the ground-state conformers found here for $[CS'p-H]^-$ and $[US'p-H]^-$. However, in an attempt to characterize the conformation of the mononucleotide, they calculated the deprotonated uridine-5'-methyl phosphate with an ammonium (NH_4^+) counterion. They found that the optimized ground-state structure exhibits a C2' *endo* conformation for the ribose and *anti* conformation for the nucleobase, and the 3'-hydroxyl hydrogen atom forms an intramolecular hydrogen bond with the oxygen atom of the 2'-hydroxyl group, while the deprotonated dioxo group is hydrogen bonded to the NH_4^+ counterion to neutralize the negative charge of the phosphate group. This is in contrast to the C3' *endo* conformation of the ribose and the orientations of the two hydrogen bonding interactions of the phosphate moiety and the 2'- and 3'-hydroxyl groups of the ground-state conformer of $[US'p-H]^-$ found here. Changes in the conformations of the deprotonated DNA and RNA mononucleotides induced by the binding of cation(s) are being explored and will be the subject of future publications. The IRMPD action spectra of $[CS'p-H]^-$ and $[US'p-H]^-$ exhibit similar features that are slightly broader and less resolved than those observed in the linear IR spectra of cytidine and uridine in aqueous solution. Nonetheless, the good agreement between the two techniques suggests that the conformations of the ribose and nucleobase of $[CS'p-H]^-$ and $[US'p-H]^-$ accessed in our experiments are similar to those sampled under aqueous conditions.

Previously, Maître and co-workers examined the conformation of deprotonated adenosine 3',5'-cyclic monophosphate $[cAMP-H]^-$ using similar techniques as employed in the present work.³⁵ The ground-state conformation they found for $[cAMP-H]^-$ exhibits a similar conformation to the AC3_3 conformer found here for $[AS'p-H]^-$, where the ribose and nucleobase are in C3' *endo* and *anti* conformations, respectively, the phosphoester oxygen atom points below the plane of the ribose, and the 2'-hydroxyl hydrogen atom is hydrogen bonded to the 3'-hydroxyl oxygen atom. The difference between these two structures lies in the orientation of the phosphate moiety, where in the cyclic structure the phosphate moiety forms a covalent phosphoester bond with the 3'-hydroxyl group and maintains the deprotonated dioxo group. The only dissociation pathway observed upon IRMPD of $[cAMP-H]^-$ results from glycosidic bond cleavage, producing the deprotonated adenine anion, $[Ade-H]^-$. Clearly, cyclization of the phosphate backbone and the 3'-hydroxyl group stabilizes the phosphate ester bonds, as the cleavage of the phosphoester bond resulting in the formation of the metaphosphate anion, PO_3^- , was observed as the major IRMPD pathway for the RNA mononucleotides examined here. In addition, two minor dissociation pathways were also observed for the deprotonated

RNA mononucleotides examined here, resulting in the formation of $[X5'p\text{-Nuc-H}]^-$ and $[H_2PO_4]^-$, while the deprotonated adenine anion pathway was completely absent. The lack of additional IRMPD dissociation pathways exhibited in their work also led to the appearance of just four intense and two weak bands in the IRMPD action spectrum of $[cAMP\text{-H}]^-$, while additional peaks that are present in the theoretical spectra are only visible in the measured spectrum upon 10 times magnification.

CONCLUSIONS

The gas-phase conformations of the four deprotonated RNA mononucleotides have been examined in this work by IRMPD action spectroscopy over the IR fingerprint region extending from ~ 600 to 1800 cm^{-1} . Comparison of the measured IRMPD action spectra with the linear IR spectra of the stable low-energy conformations of these species calculated at the B3LYP/6-311+G(d,p) level of theory allows the conformations accessed in the experiments to be identified. In the most stable conformations found for $[A5'p\text{-H}]^-$, $[C5'p\text{-H}]^-$, and $[U5'p\text{-H}]^-$, the ribose is in a *C3'* *endo* conformation and the nucleobase is in an *anti* conformation. These structures are stabilized by an intramolecular hydrogen bond between one of the oxo oxygen atoms of the deprotonated phosphate moiety and the 3'-hydroxyl hydrogen atom of the ribose moiety, while another intermolecular hydrogen bond is formed between the 2'-hydroxyl hydrogen and 3'-hydroxyl oxygen atoms, and the phosphate ester oxygen atom points above the plane of the ribose moiety. In the most stable structure found for $[G5'p\text{-H}]^-$, the ribose is also in a *C3'* *endo* conformation, while the nucleobase is in a *syn* conformation. The oxo oxygen atoms of the deprotonated phosphate moiety are stabilized by hydrogen bonding interactions with the 3'-hydroxyl and C2 amino hydrogen atoms of the ribose and nucleobase moieties, respectively, while the 2'-hydroxyl hydrogen and the 3'-hydroxyl oxygen atoms form a third intramolecular hydrogen bond, and the phosphate ester oxygen atom points below the plane of the ribose moiety. Additional stable low-energy structures were also found for each of the deprotonated RNA mononucleotides that retain the *C3'* *endo* and *anti* (*syn*) conformations and hydrogen bond to the C3' hydroxyl hydrogen atom (and 2-amino hydrogen atom in the case of $[dG5'p\text{-H}]^-$) that only differ from the ground-state conformer by the orientation of the P-OH hydroxyl group and the free oxo oxygen atom, and the orientation of the phosphate ester oxygen atom. Results from both the measured IRMPD action spectra and calculated linear IR spectra suggest that the spectral features in the region from 1300 to 1800 cm^{-1} are similar enough for all of the stable low-energy conformers calculated here that they cannot be effectively used to identify or eliminate the presence of different conformers in the experiments. However, spectral features in the region from 600 to 1300 cm^{-1} exhibit broad and somewhat diagnostic bands where the calculated frequencies from multiple stable low-energy conformers are well matched to the measured IRMPD action spectra, suggesting that multiple low-energy conformers were accessed in the experiments. This is not really surprising because the ions probed in the current work have a room temperature internal energy distribution. These findings suggest that the deprotonated phosphate group of the RNA mononucleotides is flexible and dynamic such that its conformation can be varied to a moderate extent without significant loss in stability. The results presented here are highly

parallel to those found for the deprotonated DNA mononucleotides, in particular the conformations of the deprotonated RNA mononucleotides accessed in the experiments where the most significant difference from the DNA analogues is the additional hydrogen bonding interaction between the 2'- and 3'-hydroxyl groups. However, the additional hydrogen bonding interaction provides stabilization to the overall structure such that fewer stable low-energy conformers were accessed in the experiments for all four deprotonated RNA mononucleotides as compared to the analogous deprotonated DNA mononucleotides. This would suggest that the intrinsic difference between the DNA and RNA mononucleotides is most likely not due to their relative conformations but due to the change in their chemical properties induced by the different substituents at the C2' position. This can be realized by comparing the difference in the IRMPD pathways of $[dX5'p\text{-H}]^-$ and $[X5'p\text{-H}]^-$, where onsets for the deprotonated nucleobase anions, $[Nuc\text{-H}]^-$, were not observed for any of the four deprotonated RNA mononucleotides, but were observed as very minor dissociation products in the IRMPD of the $[dA5'p\text{-H}]^-$, $[dC5'p\text{-H}]^-$, and $[dT5'p\text{-H}]^-$ systems. Similar results were also obtained using energy resolved CID⁴⁷ and UV photodissociation^{48–50} techniques, where the onset of the $[Nuc\text{-H}]^-$ pathway for $[X5'p\text{-H}]^-$ requires higher energy and is observed as low abundance dissociation species.

ASSOCIATED CONTENT

Supporting Information

Full citation for refs 14 and 44. A detailed discussion of the stable low-energy structures for each of the four deprotonated RNA mononucleotides optimized at the B3LYP/6-311+G(d,p) level of theory. Vibrational modes assigned to the measured IRMPD action spectra by comparison to the calculated linear IR spectra for all four deprotonated RNA mononucleotides. Figures comparing the relative 0 K enthalpies and 298 K Gibbs free energies calculated at the B3LYP, B3P86, M06, and MP2(full) levels of theory for the ground-state and stable low-energy conformers, excluding and including hydroxyl rotamers, for $[X5'p\text{-H}]^-$. Figures showing B3LYP/6-311+G(d,p) structures and MP2(full)/6-311+G(2d,2p) relative stabilities of all stable low-energy conformers of the four deprotonated RNA mononucleotides including hydroxyl rotamers and *C3'* *endo* and *anti* conformers of $[G5'p\text{-H}]^-$. Figures comparing the measured IRMPD action spectra to the linear IR spectra calculated for the analogous *syn* conformers of $[A5'p\text{-H}]^-$, $[C5'p\text{-H}]^-$, and $[U5'p\text{-H}]^-$. This material is available free of charge via the Internet at <http://pubs.acs.org>.

AUTHOR INFORMATION

Corresponding Author

*E-mail: mrodgers@chem.wayne.edu. Phone: (313)577-2431.

Notes

The authors declare no competing financial interest.

ACKNOWLEDGMENTS

Financial support for this work was provided by the National Science Foundation, grants PIRE-0730072 and CHE-0911191. We would also like to thank WSU C&IT for computer time and support. This work is part of the research program of FOM, which is financially supported by the Nederlandse Organisatie voor Wetenschappelijk Onderzoek (NWO). The skillful assistance of the FELIX staff is gratefully acknowledged.

■ REFERENCES

- (1) Pezzano, H.; Podo, F. Structure of Binary Complexes of Mono- and Polynucleotides with Metal Ions of the First Transition Group. *Chem. Rev.* **1980**, *80*, 365–401.
- (2) Eaton, B. E.; Pieken, W. A. Ribonucleosides and RNA. *Annu. Rev. Biochem.* **1995**, *64*, 837–863.
- (3) Cantoni, G. L. Biological Methylation. Selected Aspects. *Annu. Rev. Biochem.* **1975**, *44*, 435–451.
- (4) Grewal, S. I.; Rice, J. C. Regulation of Heterochromatin by Histone Methylation and Small RNAs. *Curr. Opin. Cell Biol.* **2004**, *16*, 230–238.
- (5) Mann, M. R.; Bartolomei, M. S. Epigenetic Reprogramming in the Mammalian Embryo: Struggle of the Clones. *Genome Biol.* **2002**, *3*, reviews1003–reviews1003.4.
- (6) Chen, R. Z.; Pettersson, U.; Beard, C.; Jackson-Grusby, L.; Jaenisch, R. DNA Hypomethylation Leads to Elevated Mutation Rates. *Nature* **1998**, *395*, 89–93.
- (7) Cox, M. M.; Nelson, D. L. *Lehninger Principles of Biochemistry*, 3rd ed.; W.H. Freeman: New York, 2004; Chapter 10.
- (8) Hardie, D. G. The AMP-Activated Protein Kinase Cascade: The Key Sensor of Cellular Energy Status. *Endocrinology* **2003**, *144*, 5179–5183.
- (9) Ni, L.; Sun, M.; Yu, H.; Chokhawala, H.; Chen, X.; Fisher, A. J. Cytidine 5'-Monophosphate (CMP)-Induced Structural Changes in a Multifunctional Sialyltransferase from *Pasteurella multocida*. *Biochemistry* **2006**, *45*, 2139–2148.
- (10) Qiao, Y.; Jian, F.; Bai, Q. Bioconjugation of Zirconium Uridine Monophosphate: Application to Myoglobin Direct Electrochemistry. *Biosens. Bioelectron.* **2008**, *23*, 1244–1249.
- (11) Callahan, J. W.; Jones, C. S.; Davidson, D. J.; Shankaran, P. The Active Site of Lysosomal Sphingomyelinase: Evidence for the Involvement of Hydrophobic and Ionic Groups. *J. Neurosci. Res.* **1983**, *10*, 151–163.
- (12) Oomens, J.; van Roij, A. J. A.; Meijer, G.; von Helden, G. Gas-phase Infrared Photodissociation Spectroscopy of Cationic Polyaromatic Hydrocarbons. *Astrophys. J.* **2000**, *542*, 404–410.
- (13) Valle, J. J.; Eyler, J. R.; Oomens, J.; Moore, D. T.; van der Meer, A. F. G.; von Helden, G.; Meijer, G.; Hendrickson, C. L.; Marshall, A. G.; Blakney, G. T. Free Electron Laser-Fourier Transform Ion Cyclotron Resonance Mass Spectrometry Facility for Obtaining Infrared Multiphoton Dissociation Spectra of Gaseous Ions. *Rev. Sci. Instrum.* **2005**, *76*, 023103.
- (14) Maître, P.; Caer, S. L.; Simon, A.; Jones, W.; Lemaire, J.; Mestdagh, H. N.; Heninger, M.; Mauclaire, G.; Boissel, P.; Prazeres, R.; et al. Ultrasensitive Spectroscopy of Ionic Reactive Intermediates in the Gas Phase Performed with the First Coupling of an IR FEL with an FTICR-MS. *Nucl. Instrum. Methods Phys. Res., Sect. A* **2003**, *507*, 541–546.
- (15) Bakker, J. M.; Besson, T.; Lemaire, J.; Scuderi, D.; Maître, P. Gas-Phase Structure of a π-Allyl-Palladium Complex: Efficient Infrared Spectroscopy in a 7 T Fourier Transform Mass Spectrometer. *J. Phys. Chem. A* **2007**, *111*, 13415–13424.
- (16) MacAleese, L.; Simon, A.; McMahon, T. B.; Ortega, J. M.; Scuderi, D.; Lemaire, J.; Maître, P. Mid-IR Spectroscopy of Protonated Leucine Methyl Ester Performed with an FTICR or a Paul Type Ion-Trap. *Int. J. Mass Spectrom.* **2006**, *249/250*, 14–20.
- (17) Abo-Riziq, A.; Crews, B. O.; Compagnon, I.; Oomens, J.; Meijer, G.; von Helden, G.; Kabeláč, M.; Hobza, P.; de Vries, M. S. The Mid-IR Spectra of 9-Ethyl Guanine, Guanosine, and 2'-Deoxyguanosine. *J. Phys. Chem. A* **2007**, *111*, 7529–7536.
- (18) Lucas, B.; Grégoire, G.; Maître, P.; Glotin, F.; Schermann, J. P.; Desfrançois, C. Infrared Multiphoton Dissociation Spectroscopy of Protonated N-Acetylalanine and Alanylhistidine. *Int. J. Mass Spectrom.* **2005**, *243*, 105–113.
- (19) Polfer, N. C.; Oomens, J.; Suhai, S.; Paizs, B. Spectroscopic and Theoretical Evidence for Oxazolone Ring Formation in Collision-Induced Dissociation of Peptides. *J. Am. Chem. Soc.* **2005**, *127*, 17154–17155.
- (20) Polfer, N. C.; Oomens, J.; Dunbar, R. C. IRMPD Spectroscopy of Metal-Ion/Tryptophan Complexes. *Phys. Chem. Chem. Phys.* **2006**, *8*, 2744–2751.
- (21) Forbes, M. W.; Bush, M. F.; Polfer, N. C.; Oomens, J.; Dunbar, R. C.; Williams, E. R.; Jockusch, R. A. Infrared Spectroscopy of Arginine Cation Complexes: Direct Observation of Gas-Phase Zwitterions. *J. Phys. Chem. A* **2007**, *111*, 11759–11770.
- (22) Armentrout, P. B.; Rodgers, M. T.; Oomens, J.; Steill, J. D. Infrared Multiphoton Dissociation Spectroscopy of Cationized Serine: Effects of Alkali-Metal Cation Size on Gas-Phase Conformation. *J. Phys. Chem. A* **2008**, *112*, 2248–2257.
- (23) Armentrout, P. B.; Rodgers, M. T.; Oomens, J.; Steill, J. D. Infrared Multiphoton Dissociation Spectroscopy of Cationized Threonine: Effects of Alkali-Metal Cation Size on Gas-Phase Conformation. *J. Phys. Chem. A* **2008**, *112*, 2258–2267.
- (24) Citir, M.; Stennett, E. M. S.; Oomens, J.; Steill, J. D.; Rodgers, M. T.; Armentrout, P. B. Infrared Multiple Photon Dissociation Spectroscopy of Cationized Cysteine: Effects of Metal Cation Size on Gas-Phase Conformation. *Int. J. Mass Spectrom.* **2010**, *297*, 9–17.
- (25) Correia, C. F.; Balaj, P. O.; Scuderi, D.; Maitre, P.; Ohanessian, G. Vibrational Signatures of Protonated, Phosphorylated Amino Acids in the Gas Phase. *J. Am. Chem. Soc.* **2008**, *130*, 3359–3370.
- (26) Oomens, J.; Steill, J. D.; Redlich, B. Gas-Phase IR Spectroscopy of Deprotonated Amino Acids. *J. Am. Chem. Soc.* **2009**, *131*, 4310–4319.
- (27) Dunbar, R. C.; Hopkinson, A. C.; Oomens, J.; Siu, C. K.; Siu, K. W. M.; Steill, J. D.; Verkerk, U. H.; Zhao, J. Conformation Switching in Gas-Phase Complexes of Histidine with Alkaline Earth Ions. *J. Phys. Chem. B* **2009**, *113*, 10403–10408.
- (28) Rijs, A. M.; Kabeláč, M.; Abo-Riziq, A.; Hobza, P.; de Vries, M. S. Isolated Gramicidin Peptides Probed by IR Spectroscopy. *ChemPhysChem* **2011**, *12*, 1816–1821.
- (29) Salpin, J.-Y.; Guillamont, S.; Tortajada, J.; MacAleese, L.; Lemaire, J.; Maître, P. Infrared Spectra of Protonated Uracil, Thymine and Cytosine. *ChemPhysChem* **2007**, *8*, 2235–2244.
- (30) Nei, Y.-w.; Akinyemi, T. E.; Steill, J. D.; Oomens, J.; Rodgers, M. T. Infrared Multiple Photon Dissociation Action Spectroscopy of Protonated Uracil and Thiouracils: Effects of Thiolacto-Substitution on Gas-Phase Conformation. *Int. J. Mass Spectrom.* **2010**, *297*, 139–151.
- (31) Nei, Y.-w.; Akinyemi, T. E.; Kaczan, C. M.; Steill, J. D.; Berden, G.; Oomens, J.; Rodgers, M. T. Infrared Multiple Photon Dissociation Action Spectroscopy of Sodiated Uracil and Thiouracils: Effects of Thiolacto-Substitution on Gas-Phase Conformation. *Int. J. Mass Spectrom.* **2011**, *308*, 191–202.
- (32) Crampton, K. T.; Rathur, A. I.; Nei, Y.-w.; Berden, G.; Oomens, J.; Rodgers, M. T. Protonation Preferentially Stabilizes Minor Tautomers of the Halouracils: IRMPD Action Spectroscopy and Theoretical Studies. *J. Am. Soc. Mass Spectrom.* **2012**, *23*, 1469–1478.
- (33) Oomens, J.; Moehlig, A. R.; Morton, T. H. Infrared Multiple Photon Dissociation (IRMPD) Spectroscopy of the Proton-Bound Dimer of 1-Methylcytosine in the Gas Phase. *J. Phys. Chem. Lett.* **2010**, *1*, 2891–2897.
- (34) Martens, S. M.; Marta, R. A.; Martens, J. K.; McMahon, T. B. Tridentate Ionic Hydrogen-Bonding Interactions of the 5-Fluorocytosine Cationic Dimer and Other 5-Fluorocytosine Analogue Characterized by IRMPD Spectroscopy and Electronic Structure Calculations. *J. Phys. Chem. A* **2011**, *115*, 9837–9844.
- (35) Chiavarino, B.; Crestoni, M. E.; Fornarini, S.; Lanucara, F.; Lemaire, J.; Maître, P.; Scuderi, D. Infrared Spectroscopy of Isolated Nucleotides. 1. The Cyclic 3',5'-Adenosine Monophosphate Anion. *Int. J. Mass Spectrom.* **2008**, *270*, 111–117.
- (36) Salpin, J.-Y.; Gamiette, L.; Tortajada, J.; Besson, T.; Maître, P. Structure of Pb²⁺/dCMP and Pb²⁺/CMP Complexes as Characterized by Tandem Mass Spectrometry and IRMPD Spectroscopy. *Int. J. Mass Spectrom.* **2011**, *304*, 154–164.
- (37) Salpin, J.-Y.; Guillaumont, S.; Ortiz, D.; Tortajada, J.; Maître, P. Direct Evidence for Tautomerization of the Uracil Moiety within the Pb²⁺/Uridine-5'-monophosphate Complex: A Combined Tandem

Mass Spectrometry and IRMPD Study. *Inorg. Chem.* **2011**, *50*, 7769–7778.

(38) Gabelica, V.; Rosu, F.; De Pauw, E.; Lemaire, J.; Gillet, J.-C.; Pouilly, J.-C.; Lecomte, F.; Grégoire, G.; Schermann, J.-P.; Desfrançois, C. Infrared Signature of DNA G-Quadruplexes in the Gas Phase. *J. Am. Chem. Soc.* **2008**, *130*, 1810–1811.

(39) Rosu, F.; Gabelica, V.; Joly, L.; Grégoire, G.; De Pauw, E. Zwitterionic *i*-Motif Structures are Preserved in DNA Negatively Charged Ions Produced by Electrospray Mass Spectrometry. *Phys. Chem. Chem. Phys.* **2010**, *12*, 13448–13454.

(40) Nei, Y.-w.; Hallowita, N.; Steill, J. D.; Oomens, J.; Rodgers, M. T. Infrared Multiple Photon Dissociation Action Spectroscopy of Deprotonated DNA Mononucleotides: Gas-Phase Conformations and Energetics. *J. Phys. Chem. A* **2013**, *117*, 1319–1335.

(41) Polfer, N. C.; Oomens, J.; Moore, D. T.; von Helden, G.; Meijer, G.; Dunbar, R. C. Infrared Spectroscopy of Phenylalanine Ag(I) and Zn(II) Complexes in the Gas Phase. *J. Am. Chem. Soc.* **2006**, *128*, 517–525.

(42) Polfer, N. C.; Oomens, J. Reaction Products in Mass Spectrometry Elucidated with Infrared Spectroscopy. *Phys. Chem. Chem. Phys.* **2007**, *9*, 3804–3817.

(43) HyperChem Computational Chemistry Software Package, version 5.0; Hypercube Inc: Gainesville, FL, 1997.

(44) Frisch, M. J.; Trucks, G. W.; Schlegel, H. B.; Scuseria, G. E.; Robb, M. A.; Cheeseman, J. R.; Scalmani, G.; Barone, V.; Mennucci, B.; Petersson, G. A.; et al. Gaussian 09, revision A.1; Gaussian, Inc.: Wallingford, CT, 2009. See the Supporting Information for the full reference.

(45) Fales, B. S.; Fujamade, N. O.; Nei, Y.-w.; Oomens, J.; Rodgers, M. T. Infrared Multiple Photon Dissociation Action Spectroscopy and Theoretical Studies of Diethyl Phosphate Complexes: Effects of Protonation and Sodium Cationization on Structure. *J. Am. Soc. Mass Spectrom.* **2011**, *22*, 81–92.

(46) Fales, B. S.; Fujamade, N. O.; Oomens, J.; Rodgers, M. T. Infrared Multiple Photon Dissociation Action Spectroscopy and Theoretical Studies of Triethyl Phosphate Complexes: Effects of Protonation and Sodium Cationization on Structure. *J. Am. Soc. Mass Spectrom.* **2011**, *22*, 1862–1871.

(47) Ho, Y.; Kebarle, P. Studies of the Dissociation Mechanisms of Deprotonated Mononucleotides by Energy Resolved Collision-Induced Dissociation. *Int. J. Mass Spectrom. Ion Processes* **1997**, *165/166*, 433–455.

(48) Brøndsted Nielsen, S.; Andersen, J. U.; Forster, J. S.; Hvelplund, P.; Liu, B.; Pedersen, U. V.; Tomita, S. Photodestruction of Adenosine 5'-Monophosphate (AMP) Nucleotide Ions *in vacuo*: Statistical versus Nonstatistical Processes. *Phys. Rev. Lett.* **2003**, *91*, 048302-1.

(49) Aravind, G.; Antoine, R.; Klærke, B.; Lemoine, J.; Racaud, A.; Rahbek, D. B.; Rajput, J.; Dugourd, P.; Andersen, L. H. Sub-Microsecond Photodissociation Pathways of Gas Phase Adenosine 5'-Monophosphate Nucleotide Ions. *Phys. Chem. Chem. Phys.* **2010**, *12*, 3486–3490.

(50) Marcum, J. C.; Kaufman, S. H.; Weber, J. M. UV-Photo-dissociation of Non-Cyclic and Cyclic Mononucleotides. *Int. J. Mass Spectrom.* **2011**, *303*, 129–136.

(51) Riley, K. E.; Pitoňák, M.; Jurečka, P.; Hobza, P. Stabilization and Structure Calculations for Noncovalent Interactions in Extended Molecular Systems Based on Wave Function and Density Functional Theories. *Chem. Rev.* **2010**, *110*, 5023–5063.

(52) Leulliot, N.; Ghomi, M.; Scalmani, G.; Berthier, G. Ground State Properties of the Nucleic Acid Constituents Studied by Density Functional Calculations. I. Conformational Features of Ribose, Dimethyl Phosphate, Uridine, Cytidine, 5'-Methyl Phosphate-Uridine, and 3'-Methyl Phosphate-Uridine. *J. Phys. Chem. A* **1999**, *103*, 8716–8724.

(53) Leulliot, N.; Ghomi, M.; Jobic, H.; Bouloussa, O.; Baumruk, V.; Coulombeau, C. Ground State Properties of the Nucleic Acid Constituents Studied by Density Functional Calculations. 2. Comparison between Calculated and Experimental Vibrational Spectra of Uridine and Cytidine. *J. Phys. Chem. B* **1999**, *103*, 10934–10944.